

Chemical Processes in Igneous Calcium-Aluminum-rich Inclusions: A Mostly CMAS View of Melting and Crystallization

John R. Beckett

California Institute of Technology

Harold C. Connolly

*Kingsborough College, City University of New York
and American Museum of Natural History*

Denton S. Ebel

American Museum of Natural History

1. INTRODUCTION

Calcium-, aluminum-rich inclusions (CAIs) and Al-rich chondrules reflect multiple processes in many different environments. In this chapter, we consider constraints on high-temperature processes from the perspective of phase equilibria and dynamic crystallization experiments. With chondrules, whose evolution is discussed in *Lauretta et al.* (2006), it is almost axiomatic that one or more igneous events were involved in processing, so the focus of research becomes one of constraining the nature of the melting event(s). CAIs are not so simple. While many CAIs are thought to have crystallized from partially or completely molten droplets, others did not, and one of the first tasks in constraining processes involved in the evolution of an object is to decide whether or not an igneous event was involved.

Our approach is to first introduce some of the objects thought to have passed through an igneous stage at some point, without getting overly concerned with nomenclature. We then explore the application of phase equilibria to CAIs through classical phase diagrams, which are useful for predicting the order of crystallization of a cooling droplet where the system is sufficiently simple, and via computational models, which draw from both phase equilibria and thermodynamic data and can, in principle, be applied to compositionally complex liquids. The phase diagram analysis proceeds mostly from the perspective of the system CaO-MgO-Al₂O₃-SiO₂ (CMAS). Other elements (e.g., Na, Ti, Fe) are considered primarily to the extent that they affect expectations based on the phase equilibria of CMAS or can help to constrain the liquid composition, but we attempt no formal characterization of the phase relations in these more complex systems. This leads us to ignore ferromagnesian chondrules, which generally have considerable amounts of FeO, and the Fe-rich opaque assemblages, or Fremdlinge, and associated V-rich pyroxenes of CAIs (*El Goresy et al.*, 1978; *Blum et al.*, 1989) even though they may have quite a bit to say about melting events. Since the observed bulk composition may be very different from the one(s) perti-

nent to an ancient igneous event, we consider the issue of secondary alteration, albeit briefly, in section 2.

The partitioning of minor and trace elements between crystalline phases and a coexisting liquid has a negligible effect on the overall phase equilibria relative to CMAS, but the process leaves clues to the history of a CAI, and in section 3.4, we discuss experimental constraints on trace-element partitioning between crystals and CAI-like and Al-rich chondrule-like liquids. The processes of volatilization and condensation are considered in *Davis* (2006) and *Ebel* (2006) (see also *Davis and Richter*, 2004). We do consider dynamic crystallization experiments in section 3.5.

We assume the reader to have a basic working knowledge of phase equilibria and the use of phase diagrams; we introduce nomenclature for CAIs and related objects as needed and note end-member compositions of mineral solid solutions when they are first encountered. *Bowen* (1928) and *Morse* (1980), among many others, provide basic background in the interpretation of phase diagrams and their use, particularly with respect to the determination of crystallization paths. Readers are referred to the review by *Brearley and Jones* (1998) for an extensive overview of the chemistry of meteoritic minerals, including those discussed here; to *MacPherson and Huss* (2005) for background on Al-rich chondrules; and to *Grossman* (1980), *MacPherson et al.* (1988), *Grossman et al.* (1988), *Kimura et al.* (1993), *Brearley and Jones* (1998), and *MacPherson* (2004) for basic background in CAIs. *MacPherson* (2004) in particular gives a nice introduction to the essential features of CAIs, and a reading of that work will provide more than adequate preparation for this chapter.

2. CALCIUM-ALUMINUM-RICH INCLUSIONS AND ALUMINUM-RICH CHONDRULES

In this section, we first introduce a few of the targets, meteoritic materials thought to have been partially or completely molten at some point and whose bulk compositions can plausibly be treated in terms of CMAS. This is done

with motivational and not comprehensive intent since our objective is to introduce tools for analyzing the possible role of liquids in the evolution of an arbitrary meteoritic inclusion rather than summarizing assertions made about specific inclusions. For our purposes, it is the bulk composition of an object during a melting event that is the single most important discriminator of how it will respond to a particular thermal history and environment; the mineralogy, elemental fractionations in individual crystals or zoning, trace-element abundances and distributions, isotopic compositions, and the presence or absence of relict crystals all flow from this fundamental property.

Although the bulk compositions of most CAIs and many Al-rich chondrules are well described by the CMAS system, they range within the system from objects with virtually no Mg or Si to objects with only a few wt% CaO + Al₂O₃. There are large corresponding variations in mineralogy. The most aluminous of CAIs contain substantial amounts of aluminates, most commonly one or more of spinel (MgAl₂O₄), hibonite (nominally CaAl₁₂O₁₉ but frequently containing significant amounts of Ti and Mg), and/or grossite (CaAl₄O₇); rarely, corundum (Al₂O₃) or calcium monoaluminate (CaAl₂O₄) may be present. Plate 11a shows an example of a corundum-bearing inclusion, which contains substantial hibonite. There is no settled nomenclature for grossite-bearing or hibonite-rich inclusions and we will not try to impose one here. As the bulk composition becomes more Si-rich, melilite, which can usually be described quite well in CAIs as a binary solid solution between gehlenite (Ca₂Al₂SiO₇) and åkermanite (Ca₂MgSi₂O₇), becomes important (e.g., Plate 11b shows four oxide phases set in melilite). *Grossman* (1975) established a basic classification structure for relatively melilite-rich inclusions. Where the inclusion is predominately melilite with minor included spinel and perovskite (\pm hibonite), it is referred to as a type A. Most type As have a porous structure and are called “fluffy” or FTA. These are generally not thought to have crystallized from a melt, but some type As have a compact form, and generally rounded shapes. These are referred to as “compact” type As, or CTAs, an example of which is shown in Plate 11c. With additional Mg and Si in the bulk composition, fassaite, describable in CAIs as Ca(Mg,Al,Ti³⁺,Ti⁴⁺)(Al,Si)₂O₆ and anorthite (nominally CaAl₂Si₂O₈) become important. Plate 11d is an example of a classic “type B1” CAI, which is characterized by a coarse-grained, melilite-rich mantle surrounding a core composed of melilite, spinel, fassaite, and anorthite. Type B2 inclusions (Plate 11e,f) have the same mineralogy but lack the melilite-rich mantle. A few type B3 inclusions, which contain significant amounts of forsterite in addition to melilite, have also been described. These objects carry an importance far beyond their sparse numbers because they frequently display a potpourri of isotope anomalies (e.g., *Davis et al.*, 1991). Type C inclusions are similar to type B2s mineralogically, but anorthite dominates over melilite. Types B and C inclusions and CTAs are generally regarded as igneous objects.

Aluminum-rich chondrules (e.g., Plate 11g) are a broad class of objects with compositions intermediate between

those of CAIs and ferromagnesian chondrules. Olivine, orthopyroxene, and plagioclase in various ratios usually, but not always, dominate the phase assemblage. Pigeonite and clinopyroxene may be present, but melilite is absent. The bulk compositions of Al-rich chondrules are generally Mg-, Si-rich and Ca-, Al-poor relative to most CAIs but, for an operational distinction between CAIs and Al-rich chondrules, we follow *MacPherson and Huss* (2005), who noted that residual liquids produced during crystallization of bulk compositions of Si-bearing CAIs generally end up producing melilite while those of Al-rich chondrules evolve away from the melilite field and toward the stability field of olivine. *MacPherson and Huss* (2005) distinguished three types of Al-rich chondrules: (1) olivine phyric, Al-rich [Oliv] chondrules and (2) plagioclase phyric Al-rich [Plag] chondrules based on their interpretation of whether plagioclase or olivine crystallized first, and (3) Al-rich [Glass] chondrules for glass-rich objects. The term phyric is a general textural term referring to the presence of large crystals in an igneous rock set in a finer-grained groundmass or glass quenched from a liquid.

All the inclusions shown in Plate 11a–f were interpreted in terms of crystallization from a melt based on both textural and chemical arguments, but any previous existence of a liquid was inferred from compositions of the crystalline phases. There are also a few examples for which cooling rates were sufficiently rapid that the liquid quenched to glass. There is some in the Al-rich chondrule shown in Plate 11g. Plate 11h shows an example of a CAI containing glass. Glass-bearing objects described in the literature encompass most of the range of bulk compositions found for completely crystalline CAIs and Al-rich chondrules.

While we are careful to distinguish between what we call a type C inclusion and an Al-rich chondrule, the demarcation between Al-rich chondrules and ferromagnesian chondrules is left fuzzy. The original definition of *Bischoff and Keil* (1983, 1984) restricted Al-rich chondrules to bulk Al₂O₃ exceeding 10 wt% but, as *MacPherson and Huss* (2005) pointed out, this is an inherently arbitrary boundary given the continuum nature of the bulk compositions. Since we restrict attention in this chapter to objects whose igneous history can plausibly be interpreted in terms of CMAS, the lack of specific pigeonholes for Al-rich and ferromagnesian chondrules will not be problematic.

The classification of CAIs and Al-rich chondrules proceeds primarily from petrography and, particularly, the phase assemblages. This is, however, largely an expression of the bulk compositions. Figure 1 is a ternary projection designed by *MacPherson and Huss* (2005) to show, among other things, the bulk compositions of many different kinds of meteoritic inclusions. We will introduce projections below but for now this figure can simply be considered a representation of bulk composition that eliminates certain ambiguities that tend to occur in binary oxide–oxide plots. The projection of Fig. 1 works well as long as the bulk composition is not too aluminous (e.g., very rich in hibonite or spinel). Grossite-bearing inclusions, CTAs, and type B and C inclusions all plot in distinct regions in Fig. 1 and can

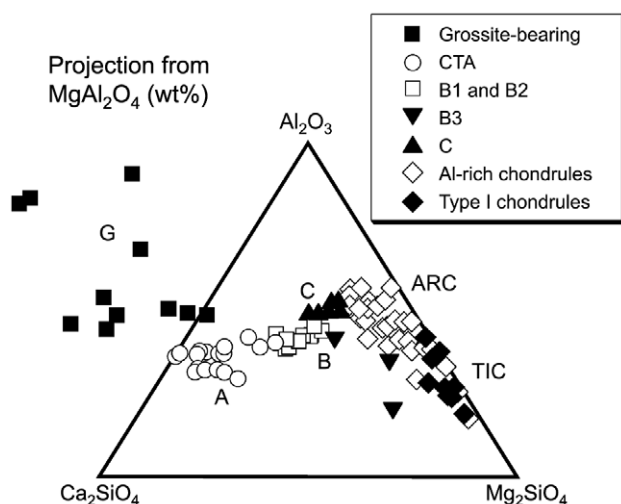


Fig. 1. Projection of bulk compositions of meteoritic inclusions from MgAl_2O_4 onto the plane defined by Mg_2SiO_4 , Al_2O_3 , and Ca_2SiO_4 . Regions occupied by different types of inclusions are indicated. A: compact type A; B: type B; C: type C; G: grossite-bearing CAIs; ARC: Al-rich chondrules; TIC: type I chondrules with less than 3 wt% each of Na_2O and FeO . Data are from *Bischoff and Keil* (1983, 1984), *Bischoff et al.* (1985, 1993), *Davis et al.* (1991), *Grossman et al.* (2000), *Jones and Scott* (1989), *Jones* (1994), *Kimura et al.* (1993), *Krot et al.* (2001), *Lin and Kimura*, (1998, 2000, 2003), *MacPherson and Huss* (2005), *Sheng et al.* (1991b), *Srinivasan et al.* (2000), *Wark* (1987), *Wark et al.* (1987), and *Weber and Bischoff* (1994, 1997).

usually be distinguished from one another based solely on the bulk composition. Aluminum-rich chondrules plot separately from the CAIs but there is substantial overlap with ferromagnesian chondrules, a reflection of the lack of a clear distinction between these two types. It should be noted that the distribution of bulk compositions, at least in this projection, is more or less continuous and yet there are sharp distinctions between different inclusion types. Investigators classified the objects based primarily on phase assemblage. This limits the range in bulk composition, but the lack of overlap is largely a consequence of the phase relations during crystallization.

Before considering the application of CMAS-based phase diagrams to meteoritic inclusions, it is important to first divide components into two camps, those present during a postulated melting event and those introduced during some later alteration event. Some meteoritic inclusions contain a lot of secondary Na_2O and/or FeO that postdates melting while in other cases, often in the same inclusion, these same oxides were present during melting (*Grossman*, 1980; *MacPherson et al.*, 1988; *Krot et al.*, 1995; *MacPherson and Huss*, 2005). In section 3.2.5, we note that phase relations based on CMAS are not badly distorted with the addition of percent level Na_2O or FeO and the usual approach at this level is to simply ignore the additional oxides and renormalize the bulk composition to CMAS. This “ignorance is bliss” approach can work well but may backfire in two ways. First, some or all of the non-CMAS oxide may have been present

in the liquid during melting. For example, even in CAIs, Na contents of igneous plagioclase are usually nonzero (e.g., *Hutcheon et al.*, 1978; *Steele et al.*, 1997), which implies that Na was present in the coexisting liquid, and they can rise to ~3 wt% Na_2O in the plagioclase from some Al-rich chondrules (*MacPherson and Huss*, 2005). Similar arguments hold for Fe and Ti oxides. Since all three oxides tend to be incompatible in the phases that crystallize at the highest temperatures, they accumulate in the residual liquid, potentially rising upon cooling to concentrations high enough to confound expectations based solely on CMAS phase relations. One should therefore monitor the concentration levels of non-CMAS components in a postulated residual liquid. Second, it is important to remember that, in general, an alteration reaction is not simply a matter of adding some new oxide to an inclusion but usually involves gains or losses of the CMAS oxides themselves. So, normalizing the bulk composition of an altered inclusion to CMAS can lead to a poor estimate of the original bulk composition. At a more sophisticated level, one can attempt to explicitly define the nature of the alteration reactions and reconstitute the primary bulk composition. For example, *MacPherson and Huss* (2005) noted that secondary nepheline preferentially replaced igneous plagioclase in some Al-rich chondrules and they estimated the prealteration bulk composition by assuming that any modal nepheline was originally plagioclase of the average composition for the inclusion. This implies a net gain in Na in the inclusion but also a net loss of Ca relative to Al and Si. *Wark* (1981), in one of his many contributions to our understanding of CAIs, noted that melilite in Allende type A inclusions was altered much more heavily than other phases. He reconstituted primary bulk compositions of mostly type A inclusions from altered ones through mass balance between melilite and the altering medium under the assumption that Al was immobile and that perovskite, hibonite, and spinel were unaffected. He found that Si generally entered the inclusions during alteration while Ca and Mg generally left. The bottom line is that if an inclusion is heavily altered, some effort must be expended to lift that veil before enlisting high-temperature phase relations in an attempt to understand the igneous history of the inclusion.

3. APPLICATION OF PHASE DIAGRAMS IN THE SYSTEM $\text{CaO-MgO-Al}_2\text{O}_3\text{-SiO}_2$

For the most part, bulk compositions of CAIs are sufficiently complex (see, e.g., *Ireland et al.*, 1991; *Weber and Bischoff*, 1994, 1997; *Lin and Kimura*, 1998; *Grossman et al.*, 2000) that the crystallization behavior cannot be described in terms of simple binary or ternary systems. There are, however, some important exceptions. We begin this section with a description of some CAIs for which simple systems have been used to deduce useful information regarding crystallization behavior or thermal history. We then consider relevant portions of the CMAS system in which all four oxide components are required for a good description of the phase relations.

3.1. Application of Binary and Ternary Phase Diagrams

3.1.1. CaO-Al₂O₃. The corundum-hibonite inclusion GR-1 is described by *MacPherson et al.* (1984a) and shown in Plate 11a. It is dominated by corundum (Al₂O₃) and low-Ti hibonite (nominally CaAl₁₂O₁₉), so the bulk composition is very close to the CaO-Al₂O₃ binary. Based on the phase diagram of *Nurse et al.* (1965), *MacPherson et al.* (1984a) noted that crystallization of hibonite and corundum from a liquid in GR-1 required temperatures in excess of 1830°C. They rationalized the observed textures in terms of melting of an original hibonite with partial distillation of Ca followed by crystallization of corundum and a second generation of hibonite. A later assessment of the CaO-Al₂O₃ binary by *Hallstedt* (1990) puts the hibonite-corundum peritectic at 1883°C, somewhat higher than given by *Nurse et al.* (1965), but this does not affect the fundamental point made by *MacPherson et al.* (1984a), that very high temperatures were required to produce GR-1 and, based on their observations, an environment in the solar nebula capable of generating such high temperatures must have existed.

3.1.2. MgO-Al₂O₃. Although no CAIs with bulk compositions on this join have been described, aluminous spinels with compositions along the join MgAl₂O₄-Al₂O₃ are encountered occasionally in which the molar Al/Mg ratio of the spinel exceeds the 2.0 expected for MgAl₂O₄ (*El Goresy et al.*, 1984; *Simon et al.*, 1994b; *Yurimoto et al.*, 2001). The stability limits of phases of known composition can sometimes provide useful constraints on thermal history. The solubility of excess Al in Mg-Al spinels is negligible below 1000°C but increases with temperature to a maximum molar Al/Mg of 20 for spinel in equilibrium with corundum and liquid at 1994°C (*Hallstedt*, 1992). The highly aluminous spinels described by *Yurimoto et al.* (2001), with Al/Mg as high as 7, require temperatures of at least ~1800°C if they formed at equilibrium. Similarly, the 10 mol% Al_{8/3}O₄ (a molecule of alumina on a 4-oxygen basis to be consistent with spinel stoichiometry) reported by *El Goresy et al.* (1984) for spinel in the rim of an Essebi inclusion would require a *minimum* temperature of formation of 1590°C according to the assessment of *Hallstedt* (1992), a condition that would have resulted in partial melting had the entire object been equilibrated at such a high temperature. Since *El Goresy et al.* (1984) interpreted the inclusion in terms of condensation/evaporation, this implies that the spinel was either exotic or that nonequilibrium processes were involved.

3.1.3. CaO-Al₂O₃-SiO₂. *Ivanova et al.* (2002) described a fragment of an originally spheroidal inclusion containing calcium monoaluminate (CaAl₂O₄), an as-yet-unnamed mineral, from the CH chondrite Northwest Africa (NWA) 470. The inclusion, labeled E1-005, is modally zoned outward from a core containing ragged grossite (CaAl₄O₇) with interstitial melilite, very nearly pure gehlenite in composition, and perovskite, to a region dominated by CaAl₂O₄ enclosing melilite and perovskite with minor grossite, to an area composed essentially of grossite and late perovskite and,

finally, a mantle of essentially monomineralic melilite. *Ivanova et al.* (2002) compared texturally inferred crystallization sequences with those predicted for crystallization of an initially molten droplet from the outside inward using the phase diagram for the CaO-Al₂O₃-SiO₂ (CAS) system. They concluded that the outer melilite rim was inconsistent with crystallization from a melt corresponding to the bulk inclusion. If, however, the melilite mantle was removed from the analysis, then bulk silica was cut in half and a crystallization sequence of grossite → CaAl₂O₄ (with grossite in a reaction relationship) → melilite made crystallization from a liquid more plausible. At first glance, the analysis appears flawed because, although the inclusion has virtually no Mg, there is considerable Ti. *Ivanova et al.* (2002) give the bulk TiO₂ as ~6 wt% and because grossite, CaAl₂O₄, and melilite are virtually Ti-free, residual liquids produced as these phases crystallized would have become progressively more titaniferous until perovskite finally appeared. In other words, unless most of the perovskite is relict, seemingly unlikely given its petrographic context, the appropriate system for discussing the phase equilibria of E1-005 is CaO-Al₂O₃-SiO₂-TiO_x and not CAS. To the extent Ti affects the topology of the phase diagram and/or positions of boundary curves relative to CAS, ignoring Ti could lead to erroneous predictions of crystallization sequences and therefore incorrect conclusions regarding whether or not the observed phases crystallized from a melt. Certainly, the crystallization sequence of an otherwise CAS liquid with 6 wt% MgO would generally bear little resemblance to the crystallization sequence expected for a melt in the ternary CAS. Unfortunately, there are no experimental data for the phase equilibria of a bulk composition corresponding to that of E1-005, and therefore no direct test of the influence of Ti on the phase relations. Data are available, however, for the ternaries Al₂O₃-SiO₂-TiO₂ (*Kirschen et al.*, 1999), CaO-SiO₂-TiO₂ (*DeVries et al.*, 1955), CaO-Al₂O₃-TiO₂ (*Imlach and Glasser*, 1968), and three silica-rich joins, Anorthite (CaAl₂Si₂O₈)-Titanite (CaSiTiO₅)-Silica, Anorthite-Titanite-Wollastonite (CaSiO₃), and Anorthite-Titanite-Silica with 30 wt% Wollastonite, whose compositions also lie within the CaO-Al₂O₃-SiO₂-TiO₂ system (*Agamawi and White*, 1953, 1954a,b). For these data, there are two consistent patterns as TiO₂ is added to a base composition in CAS. First, the liquidus temperature decreases, for 6 wt% TiO₂ by anywhere from 10° to 115°C. Second, and most important, boundary curves involving two Ti-free crystalline phases with compositions in CAS tend, as TiO₂ is added to the liquid, to point toward TiO₂. This means that if the composition of a multiply saturated liquid is projected back to CAS from TiO₂ (i.e., TiO₂ is ignored), it has essentially the same position it would have had in the Ti-free system. An exception occurs for the calcic aluminates Ca₃Al₂O₆ and Ca₁₂Al₁₄O₃₃, the projected equilibria being more calcic than expected based on CaO-Al₂O₃, but these phases are not observed in CAIs. Thus, the addition of Ti affects the properties of the liquid, leading to some suppression of the liquidus temperature but to first order, it has no effect on relative stabilities of the

Ti-free crystalline phases. It should be remembered that this assertion has not been tested for low-silica compositions in the CaO-Al₂O₃-SiO₂-TiO₂ system relevant to grossite- and CaAl₂O₄-bearing CAIs but, in the absence of such a study, the approach used by *Ivanova et al.* (2002) of ignoring the effect of Ti on the order of crystallization seems reasonable provided a Ti-rich phase other than rutile is not on the liquidus. The caveat arises from the fact that fractionation of a Ti-rich phase containing significant amounts of another oxide (e.g., CaO in perovskite) depletes the liquid in that oxide relative to the bulk composition, thereby potentially affecting predictions concerning the identity of a second crystallizing phase. In E1-005, however, perovskite is interstitial (*Ivanova et al.*, 2002) and there is no other phase with significant Ti. A final caveat concerning the use of CAS is that if the melt contains significant Mg as well as Ti, this allows the coupled substitution $Mg^{2+} + Ti^{4+} = 2Al^{3+}$ in hibonite and stabilization of hibonite relative to grossite (e.g., *Beckett and Stolper*, 1994). CAS should probably not be used if hibonite is present and bulk MgO exceeds a few tenths of a wt%. *Weber and Bischoff* (1994) used the phase relations for CaO-Al₂O₃-SiO₂ taken from *Gentile and Foster* (1963) to predict crystallization sequences for grossite-bearing inclusions with 1–2 wt% MgO but properly cautioned that considerable uncertainty accrued through the presence of minor elements. We discuss these inclusions in section 3.2.

3.1.4. CaO-Al₂O₃-MgO. *MacPherson et al.* (1983) described BB-2, a spinel-hibonite spherule from Murchison, and *Simon et al.* (1994b) described a grossite-bearing spherule with a very similar bulk composition. Both inclusions have ~3 wt% TiO₂ tied up in perovskite, but virtually no Si. *Lin and Kimura* (2000) described a spinel-hibonite-grossite spherule included in a type B inclusion and *Yurimoto et al.* (2001) gave a preliminary description of an ultra-refractory inclusion with hibonite, spinel, perovskite, and an alumina phase. In all four studies, the system CaO-Al₂O₃-MgO (CAM) was used as a basis for discussing the phase relations and the potential for the inclusions having crystallized from a liquid. *MacPherson et al.* (1983) used a compilation of data from *Rankin and Merwin* (1916), *Gentile and Foster* (1963), *Nurse et al.* (1965), and *Rao* (1968). *Simon et al.* (1994b) and *Lin and Kimura* (2000) used the thermodynamic model of *Berman* (1983) to construct a CAM phase diagram. This model is discussed in section 3.3.1 but for now it can effectively be considered an alternative phase diagram for CAM that draws on a somewhat larger set of data sources than used by *MacPherson et al.* (1983). A more recent model for the system (*Hallstedt*, 1995) generates a reasonably similar phase diagram but the discovery of two new phases, Ca₂Mg₂Al₂₈O₄₆ and CaMg₂Al₁₆O₂₇, with compositions between spinel and hibonite (*Göbbels et al.*, 1995) postdates *Hallstedt's* (1995) assessment and suggests that the phase diagram may need revision. The two new phases have not been observed in CAIs, possibly speaking to very limited stability as Si and/or Ti is added to the system. According to *de Aza et al.* (2000), the phases have adjacent

stable primary phase fields bounded by those of hibonite, grossite, and spinel with a configuration such that liquids coexisting simultaneously with hibonite, grossite, and spinel are unstable. Experimental confirmation for the new phases is desirable and also for the *de Aza et al.* corundum and hibonite primary phase fields, which extend to considerably more magnesian compositions than obtained by previous workers. The *de Aza et al.* phase diagram also should not be used without correction of its numerous violations of Schreinemaker's rule (*Zen*, 1966). Finally, it should be noted that information on the effect of Ti on the phase relations relative to pure CAM is limited to the ternaries CaO-MgO-TiO₂ (*Kirschen and de Capitani*, 1999) and CaO-Al₂O₃-TiO₂ (*Imlach and Glasser*, 1968). For liquids in CaO-MgO-TiO₂ with less than ~10 wt% TiO₂, the position of the pericline (MgO)-lime-liquid boundary curve projected from TiO₂ onto CaO-MgO is within 1 wt% of its position on the Ti-free binary CaO-MgO although the temperature decreases by as much as ~150°C. This is consistent with the theme presented in the preceding section that additions of Ti tend to reduce liquidus temperatures but affect Ti-free crystalline phases similarly. Since hibonite can accommodate considerable amounts of Ti if Mg is present, it is likely that hibonite is stabilized relative to grossite, as indeed was observed by *Beckett and Stolper* (1994) in the more complex system CMAS + TiO₂ (CMAS^T). The solubility of Ti in the new phases described by *Göbbels et al.* (1995) is unknown and it is uncertain whether or not they are stable for bulk compositions relevant to CAIs.

3.2. Projections of Quaternary Phase Relations

In a projection, a composition presented in terms of one basis set of components (e.g., end-member oxides) is recast in terms of an alternative basis set. The reason for doing this is to reduce the number of dimensions for graphical depiction of a suite of compositions without too much loss of information. Projections are a basic tool used to depict compositions in multicomponent systems (e.g., *McMurdie and Insley*, 1936; *Greenwood*, 1975; *Spear*, 1993) and they have found widespread application in studies of CAIs (e.g., *Stolper*, 1982; *Stolper and Paque*, 1986; *Davis et al.*, 1991; *MacPherson and Davis*, 1993; *Beckett and Stolper*, 1994; *Lin and Kimura*, 2000; *Huss et al.*, 2001; *Krot et al.*, 2001) and Al-rich chondrules (*Sheng et al.*, 1991a; *Sheng*, 1992; *Srinivasan et al.*, 2000; *MacPherson and Huss*, 2005). There are three basic types of applications. First, projections of liquid compositions saturated with respect to one or more crystalline phases can be used to construct phase diagrams from which the primary phase field of a given bulk composition can be determined. Second, provided a phase diagram is appropriate for a given bulk composition, the liquid line of descent for equilibrium or, more usually, fractional crystallization of a liquid and hence the order of appearance of phases can be determined. A third use is to depict variations in composition for one or more groups of CAIs or glasses, usually with the idea of comparing compositions

of meteoritic materials with model predictions for condensation/volatilization trajectories, identifying possible end members for mixtures producing the observed suite of compositions, or showing differences in composition among groups of meteoritic inclusions (Stolper, 1982; Beckett and Grossman, 1988; Grossman et al., 2000; MacPherson and Huss, 2005). Figure 1 is an example of the latter.

3.2.1. Stolper's projection. Stolper (1982) was the first to popularize the use of projections to describe phase equilibria relevant to CAIs. The diagram was designed primarily for type B inclusions, for which it remains very useful (e.g., Lin and Kimura, 2000; Simon and Grossman, 2003). Later projections (e.g., Beckett and Grossman, 1988; Beckett and Stolper, 1994; MacPherson and Huss, 2005; this work) were tailored to other types of CAIs or allowed the depiction of a broader range of compositions than is possible with Stolper's (1982) projection.

Figure 2a shows the tetrahedron defined by the compositions of end member gehlenite ($\text{Ca}_2\text{Al}_2\text{SiO}_7$), anorthite ($\text{CaAl}_2\text{Si}_2\text{O}_8$), forsterite (Mg_2SiO_4), and spinel (MgAl_2O_4) (GAFS) within the tetrahedron defined by the oxides CaO, MgO, Al_2O_3 , and SiO_2 (CMAS). Any bulk composition lying inside or on the CMAS tetrahedron can be described in terms of positive amounts of CMAS oxides. Similarly, any composition lying inside or on the GAFS tetrahedron can be described in terms of positive amounts of GAFS components and, since GAFS lies within CMAS, such a composition could also be described in terms of positive amounts of CMAS oxides. In Fig. 2a, however, much of the CMAS tetrahedron lies outside the GAFS tetrahedron. All such compositions are physically realizable but if they are defined in terms of GAFS, one or more of the GAFS components will be negative. There is nothing wrong with using negative amounts of components to describe a composition.

The physical significance of the projection of a CMAS composition that lies outside the GAFS tetrahedron from MgAl_2O_4 spinel (SP) onto the plane defined by end-member compositions of gehlenite (GE), anorthite (AN), and forsterite (FO) can be seen in Fig. 2a. Consider the join Ca-Tschermaks (CaTs; $\text{CaAl}_2\text{SiO}_6$)-diopside (Di; $\text{CaMgSi}_2\text{O}_6$), which is an important binary for CAI fassaite. The compositions of both CaTs and Di lie outside the GAFS tetrahedron. To obtain a projection of Di from SP onto the plane GE-AN-FO, a line defined by the two points Di and SP is drawn and the point where this line intersects the plane defined by GE-AN-FO defines the projection point for Di. As shown in Fig. 2a, this point lies within the GE-AN-FO triangle (see also Fig. 4a of Stolper, 1982). A line drawn through spinel (SP) and CaTs also intersects the GE-AN-FO plane but the projection point lies outside the triangle. This illustrates the important concept that there is nothing sacred about projection points having to plot within the composition triangle defining the projection plane.

In the above analysis, we accepted the set of components used by Stolper without pausing to consider what constituted a valid set of components or why one should prefer one particular set of candidate end members to another.

These are two distinctly different issues to consider. (1) In general, any set of four end-member compositions within CMAS that defines a tetrahedron will generate a valid set of components and, in fact, end-member compositions lying outside CMAS are equally valid, although such components have not been used in meteoritic applications. The statement that a set of proposed compositions form a tetrahedron within or even outside CMAS is equivalent to saying that the proposed set of components must be linearly independent. Thus, the set of components MgAl_2O_4 , Al_2O_3 , Ca_2SiO_4 , and Mg_2SiO_4 selected by MacPherson and Huss (2005) provides a valid representation of CMAS compositions, but åkermanite ($\text{Ca}_2\text{MgSi}_2\text{O}_7$), gehlenite ($\text{Ca}_2\text{Al}_2\text{SiO}_7$), Ca-Tschermaks ($\text{CaAl}_2\text{SiO}_6$), and diopside ($\text{CaMgSi}_2\text{O}_6$) would be invalid because the compositions lie within the same plane, and therefore a tetrahedron cannot be constructed from them. In the latter case, the proposed components are related through the relationship åkermanite + Ca-Tschermaks = diopside + gehlenite (i.e., they are not independent). For CAI applications, some components are invariably chosen to correspond to major end-member compositions of phases that occur either in CAIs or as stable phases within CMAS, but this is not required. Any set of four independent compositions could, in principle, be selected. In a system containing five or more components, the easily visualized geometric construct usable in a quaternary system fails, but the basic constraint that all compositions of all proposed end members must be independent still holds. (2) The second issue regarding the selection of components for constructing projections depends critically on the application. In Stolper's projection, the operational objectives were to show bulk compositions of type B and C CAIs, multiply saturated liquid phase fields for such bulk compositions in which spinel and liquid coexist with one or more additional crystalline phases, the crystallization paths of such liquids, and a comparison of bulk CAI compositions with calculated condensates. Since the intent was a consideration of phase assemblages saturated with respect to spinel that is very close in composition to the end member MgAl_2O_4 for the CAIs of interest and in his experiments, Stolper (1982) chose MgAl_2O_4 spinel as one component. For the remaining three components, the choice was mostly one of convenience in presentation. Type B and C inclusions contain spinel and various amounts of melilite, fassaite, anorthite, and occasionally olivine, so likely candidates include the end-member compositions åkermanite, gehlenite, Ca-Tschermaks, diopside, anorthite, and forsterite. The only combination of three end members from this list that led to all bulk compositions of type B and C inclusions available in 1982 being projected from spinel to points within or even close to the base ternary was the one selected by Stolper (i.e., gehlenite, anorthite, and forsterite).

In CMAS, the locus of liquid compositions in equilibrium with two crystalline phases over a range of temperatures will describe a surface, and where two such surfaces intersect, they produce a space curve, which describes the compositions of liquids saturated with respect to three crys-

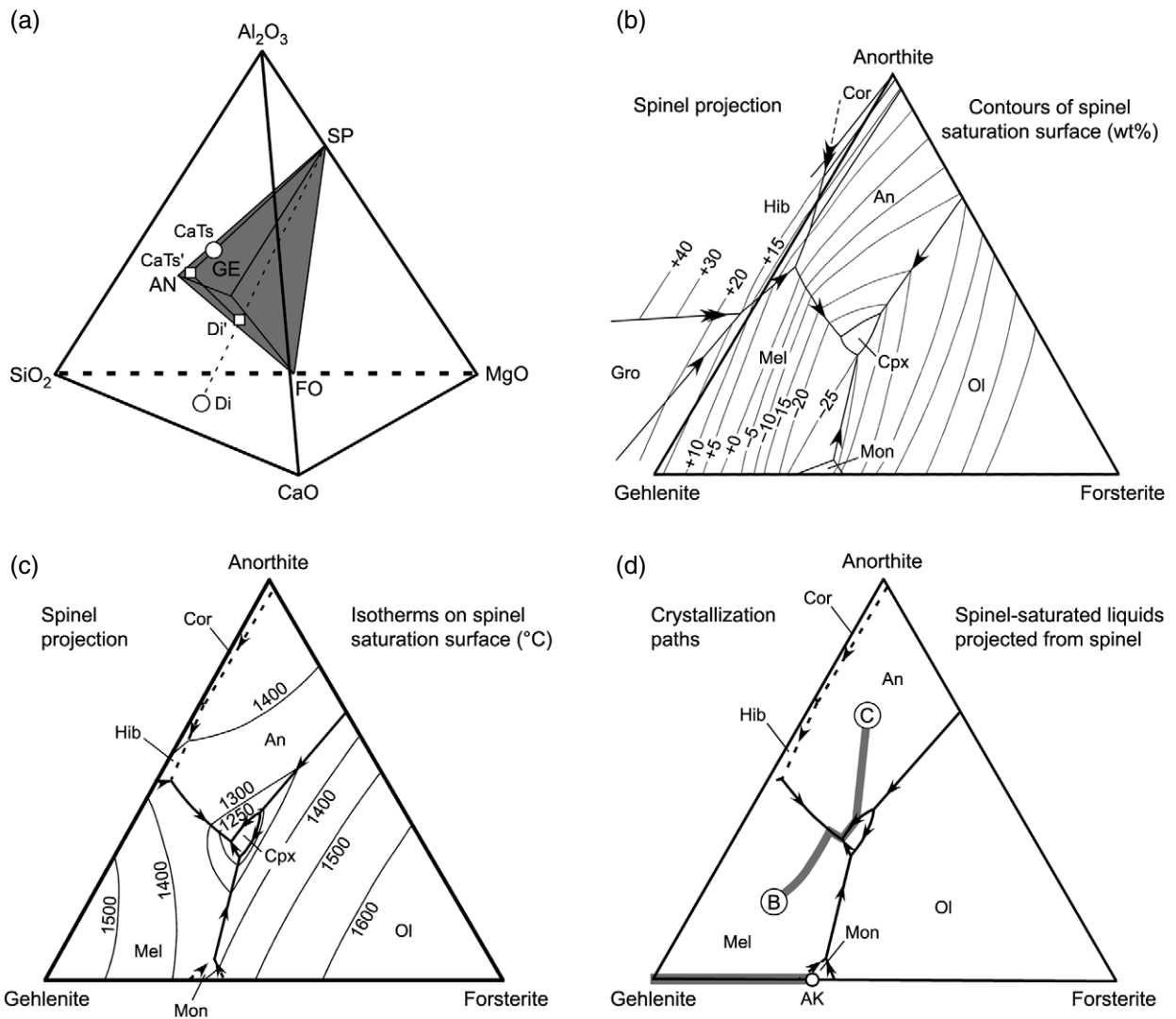


Fig. 2. *Stolper's* (1982) projection from spinel onto the plane defined by the compositions of gehlenite, anorthite, and forsterite. (a) Location of the gehlenite-anorthite-forsterite-spinel (GAFS) tetrahedron within the CMAS tetrahedron. GAFS end members gehlenite (GE), anorthite (AN), forsterite (FO), and spinel (SP) are indicated. The positions of end member diopside (Di) and Ca-Tschermaks (CaTs) and their projected positions (Di', CaTs') are also shown (squares). (b) Projection of surfaces, defined by liquid compositions in which spinel is in equilibrium with the liquid and an additional crystalline phase, from MgAl_2O_4 spinel onto the GAF plane. Each field in (b), (c), and (d) is labeled only by the identity of the additional phase as all surfaces refer to compositions of liquids that are saturated with respect to spinel. The surfaces are contoured in wt% MgAl_2O_4 above the gehlenite-anorthite-forsterite plane. Spinel-saturated liquidus phase fields are indicated for melilite (Mel), clinopyroxene (Cpx), olivine (Ol), monticellite (Mon), grossite (Gro), hibonite (Hib), corundum (Cor), and anorthite (An). The figure, after *Beckett and Stolper* (1994), is a slight modification of the projection given by *Stolper* (1982). (c) Projection of spinel-saturated liquidus surfaces, contoured in terms of temperature ($^{\circ}\text{C}$). After *Stolper* (1982). (d) Fractional crystallization paths for compositions typical of type B (point B) and type C (point C) inclusions. Phase relations after *Stolper* (1982). The projected composition of åkermanite (AK) is indicated and the melilite-åkermanite-gehlenite join shaded.

talline phases. In *Stolper's* (1982) projection, a set of surfaces saturated with respect to spinel were projected from MgAl_2O_4 spinel onto the plane defined by the compositions of gehlenite, anorthite, and forsterite. Compositions above the surface have spinel on the liquidus, the temperature above which no crystalline phases are stable; compositions on the surface have spinel and a second crystalline phase on the liquidus. If the liquid composition lies just below the surface, then the second phase will be on the liquidus. There

are big advantages to projections in describing crystallization sequences as discussed below but there are also disadvantages. Information is always lost in a projection and it is very important to first make sure that a particular projection is valid for the compositions of interest. Three-dimensional saturation surfaces disappear in projection and the three-dimensional boundary curves marking the intersections of saturation surfaces map as two-dimensional curves. The first step in deciding whether or not a particular pro-

jection is suitable for describing the crystallization behavior of a particular liquid is to determine whether or not the composition of that liquid plots within the primary liquidus phase volume of the saturating phase or on a bounding multiply saturated liquidus surface. For Stolper's projection, this is equivalent to asking if a liquid composition is on or above the saturation surface, that is, between spinel and the saturation surface. A simple way to address this is to contour the projected saturation surface in terms of the amount of the projected component, essentially a topographic map of the projected surface, and then ask whether the liquid composition of interest lies above or below the surface. Figure 2b shows the spinel saturation surface for GAFS contoured in terms of wt% of the spinel component. It is worth noting in Fig. 2b that many of the contours have negative amounts of spinel component in the liquid. It is, however, the relative amounts of spinel component in a liquid and on the saturation surface that is important in determining the liquidus phase, not whether the numbers are positive or negative. Thus, a liquid whose composition has -10 wt% spinel component that plots in projection on a -20 wt% isopleth in Fig. 2b will have spinel on the liquidus because the composition lies above the spinel liquidus saturation surface even though it has a negative amount of spinel component. One with +20 wt% spinel component that plots on the +40 wt% spinel isopleth will have some other phase on the liquidus because it plots below the spinel saturation surface even though it has a positive amount of spinel component. In general, if a liquid composition lies above the saturation surface based on the GAFS components calculated according to the method given in Stolper (1982), then the projection provides a valid representation of the crystallization behavior of the liquid as long as the saturating phase, spinel in this case, is present. If it plots below the spinel saturation surface, then some phase other than spinel is on the liquidus and Stolper's projection becomes valid only when spinel joins the instantaneously crystallizing phase assemblage. This is a vital point for the use of any projection to infer crystallization sequences in CAIs. If a liquid composition is not above the saturation surface being projected, then the projected phase is not on the liquidus and use of the projection to infer crystallization sequences is invalid.

The saturation surface identifies the phase on the liquidus for compositions lying immediately beneath the saturation surface but it says nothing about how deep that liquidus phase volume might be and, therefore, unless the composition of interest is essentially kissing the surface, the liquidus phase and crystallization behavior prior to the appearance of spinel should be determined before proceeding. For some compositions, the liquid will never actually reach the spinel saturation surface even if it projects comfortably within the GAF triangle of Fig. 2b. Stolper (1982) showed for nearly all type B1, B2, and C inclusions that the bulk compositions were on or above the spinel saturation surface and, therefore, his projection scheme was valid for determining crystallization paths of those inclusions. For some type B3 inclusions (e.g., Davis *et al.*, 1991), olivine is the liquidus phase

and early crystallization behavior for such inclusions should be determined using a suitable projection from forsterite. For type A inclusions, melilite is generally the liquidus phase.

Temperature is an important intensive variable for constraining astrophysical processes, and Stolper's (1982) projection can be used to place some constraints on what the temperatures may have been during melting and crystallization of type B and C inclusions. This derives from the fact that two crystalline phases, such as melilite and spinel, are in equilibrium with the same CMAS liquid at only one temperature (for a specific total pressure), which means it is possible to contour the spinel-saturated liquidus surface in terms of temperature (Fig. 2c); by similar reasoning, one can also contour in terms of the composition of a solid phase (e.g., Beckett *et al.*, 1999). For bulk compositions of CAIs available in 1982, minimum temperatures above which melilite is unstable, and therefore minimum peak temperatures for the inclusions if melilite crystallized from a melt, ranged from ~1240°C for compositions plotting near the fassaite + spinel field to ~1450°C for melilite-rich type B inclusions. For the average type B composition Stolper (1982) investigated experimentally, the corresponding temperature is ~1400°C and this, together with the results of dynamic crystallization experiments discussed in section 3.5, led to a widely held view that maximum temperatures experienced by type B inclusions were roughly 1400°C.

One of the most important properties of projections for the study of meteoritic inclusions is that the determination of crystallization paths and sequences in a quaternary system projected to a ternary is, in many instances, no more complicated than for a true ternary system. Consider points B and C in Fig. 2d. Point B would be typical of a type B inclusion and point C of a type C inclusion. Let's assume, as is observed for the meteoritic inclusions, that both compositions plot above the spinel saturation surface. Fractional crystallization of spinel from bulk composition B drives the liquid composition directly away from spinel until it encounters the spinel saturation surface. Since the projection in Fig. 2d is from the composition of the phase that is crystallizing (i.e., from MgAl₂O₄ spinel), bulk composition B and a residual liquid derived from B by crystallization of spinel project to the same point. Once on the spinel saturation surface, however, melilite (plus spinel) crystallize and the projected position of the residual liquid is driven away from the plane åkermanite-gehlenite (i.e. melilite)-spinel, which projects to the base of the triangle in Fig. 2d. The instantaneously crystallizing melilite becomes more åkermanitic with progressive crystallization and this leads to the curved path shown in Fig. 2d. Further crystallization drives the liquid to the melilite + anorthite + spinel + liquid boundary curve, at which point anorthite joins the instantaneously crystallizing phase assemblage. The residual liquid composition then moves down the boundary curve, in the direction away from the composition plane of the instantaneously crystallizing phase assemblage, until clinopyroxene crystallizes and the remaining liquid is consumed or the liquid leaves the spinel saturation surface. Fractional crystalliza-

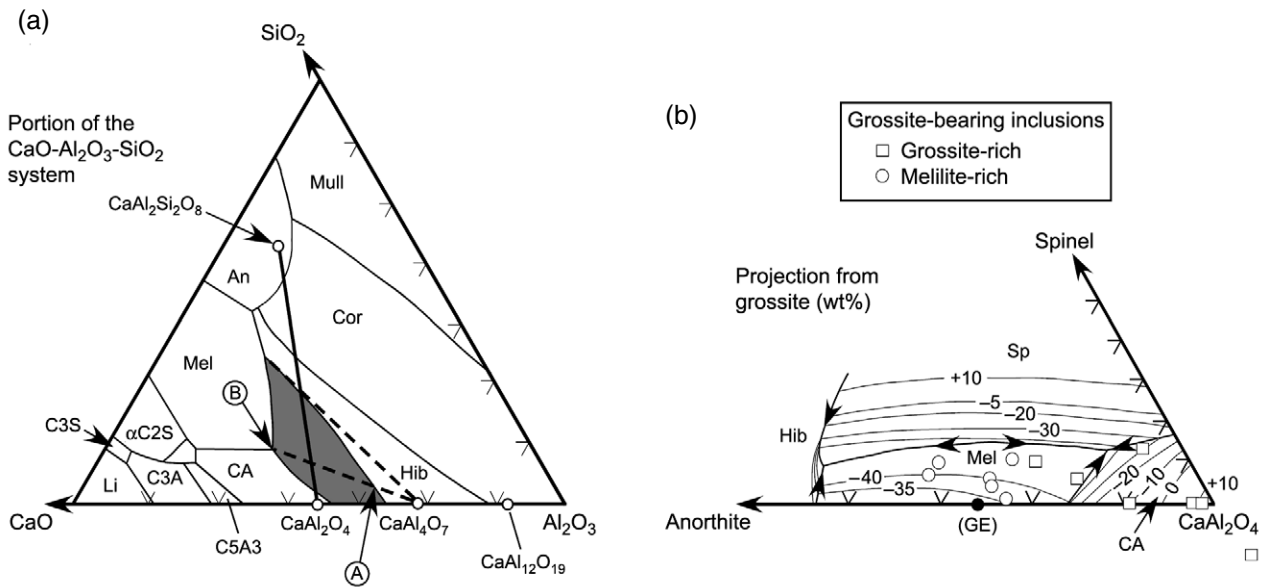


Fig. 3. Projections of liquidus-saturated phase relations in portions of CMAS. **(a)** Liquidus phase fields for a portion of the system $\text{CaO-Al}_2\text{O}_3\text{-SiO}_2$ (after *Gentile and Foster*, 1963). Two projection lines from grossite onto the join anorthite ($\text{CaAl}_2\text{Si}_2\text{O}_8$)-calcium monoaluminate (CaAl_2O_4) are indicated. Points A and B are stability limits for grossite plus liquid along one of these lines. Primary phase fields for anorthite (An), CaAl_2O_4 (CA), $\text{Ca}_5\text{Al}_6\text{O}_{14}$ (C5A3), $\text{Ca}_3\text{Al}_2\text{O}_6$ (C3A), Ca_3SiO_5 (C3S), $\alpha\text{-Ca}_2\text{SiO}_4$ (αC2S), corundum (Cor), grossite, hibonite (Hib), lime (Li), melilite (Mel), and mullite (Mull) are shown, with the grossite field shaded. For clarity, the $\beta\text{-Ca}_2\text{SiO}_4$ and grossite fields are not labeled. Tic marks are shown at 10 wt% intervals. **(b)** Projection of grossite-saturated liquidus phase fields in CMAS from CaAl_4O_7 (grossite) onto the plane defined by CaAl_2O_4 (calcium monoaluminate), MgAl_2O_4 (spinel), and $\text{CaAl}_2\text{Si}_2\text{O}_8$ (anorthite). Grossite is in a reaction relationship with the liquid along the CA-spinel-grossite boundary curve. Tic marks are shown at 10% intervals along $\text{CaAl}_2\text{O}_4\text{-CaAl}_2\text{Si}_2\text{O}_8$ and 5% intervals along $\text{CaAl}_2\text{O}_4\text{-MgAl}_2\text{O}_4$. The saturation surface is contoured in terms of wt% CaAl_4O_7 . Bulk compositions of grossite-bearing inclusions from *Weber and Bischoff* (1994) are shown as open circles (<10 wt% CaAl_4O_7 component) and open squares (>70 wt% CaAl_4O_7 component) and the projected composition of end member gehlenite (GE) is also indicated (closed circle). Melilite in grossite-bearing inclusions is highly aluminous (e.g., *Weber and Bischoff*, 1994) and compositions plot very close to GE. Coordinates for plotting points in this diagram may be determined from oxide mole fractions as CaAl_2O_4 (wt%) = $79.02(4\text{CaO} + 2\text{MgO} + 2\text{Al}_2\text{O}_3 - \text{SiO}_2)$, $\text{MgAl}_2\text{O}_4 = 142.65\text{MgO}$, $\text{CaAl}_2\text{Si}_2\text{O}_8 = 139.105\text{SiO}_2$, and $\text{CaAl}_4\text{O}_7 = 260.001(\text{Al}_2\text{O}_3\text{-CaO-MgO})$ followed by normalization to $\text{CaAl}_2\text{O}_4\text{-MgAl}_2\text{O}_4\text{-CaAl}_2\text{Si}_2\text{O}_8$. See text for data sources used in constructing the figure.

tion of C can be followed in a similar manner. Spinel crystallizes until the liquid reaches the spinel saturation surface, at which point anorthite joins the crystallizing phase assemblage and the residual liquid is driven directly away in projection from the anorthite vertex. When the residual liquid reaches the anorthite + clinopyroxene + spinel + liquid boundary curve, clinopyroxene crystallizes and the liquid evolves along the boundary curve until it reaches the melilite-anorthite-clinopyroxene-spinel invariant point. Note that the inferred crystallization paths for points B and C look just like they would have been (aside from spinel being present) had Fig. 2d been a true ternary.

3.2.2. Projections for highly aluminous systems. The Stolper projection is well posed for a discussion of phase equilibria relevant to most type B and C inclusions, but is much less useful for the often spinel-undersaturated, highly aluminous CAIs, whose compositions tend to project outside the GAF triangle to the forsterite-poor side of the anorthite-gehlenite join in Fig. 2b or of Al-rich chondrules, whose compositions generally project outside the GAF triangle to the gehlenite-poor side of the anorthite-forsterite

join. In this and the following section, we discuss projections that can be applied to some aluminous CAIs and Al-rich chondrules to infer liquidus phases and crystallization paths.

Stolper (1982) projected compositions from MgAl_2O_4 because spinel is present in type B1 and B2 CAIs on or near the liquidus and the composition of the phase is consistently close to MgAl_2O_4 in these inclusions. Similar considerations apply to projections for which spinel is not the liquidus phase, but if the liquidus phase melts incongruently, as hibonite, enstatite, and grossite do, some complications not apparent in *Stolper's* projection become important. We illustrate the principles for a two-dimensional case in Fig. 3a, which shows aluminous portions of the CAS system after *Gentile and Foster* (1963). Suppose that we are interested in projecting compositions of liquids saturated with respect to grossite and an additional crystalline phase from CaAl_4O_7 (grossite) onto the join CaAl_2O_4 (CA)- $\text{CaAl}_2\text{Si}_2\text{O}_8$ (An), which is really a description of CAS compositions in terms of grossite (CaAl_4O_7), calcium monoaluminate (CaAl_2O_4), and anorthite ($\text{CaAl}_2\text{Si}_2\text{O}_8$). Two examples are shown in

Fig. 3a via dashed line segments drawn from CaAl_4O_7 through the CA-An join. The first is drawn grazing the extreme Si-rich end of the grossite primary phase field. It intersects CA-An at the projection point for this liquid. Note that there is only one grossite-saturated liquid that projects to this point and that there are no grossite-saturated liquids whose compositions plot at more An-rich compositions along CA-An. This lack of stable liquids saturated with respect to the projecting phase is a natural consequence of projecting from the composition of an incongruently melting compound. The second dashed line in Fig. 3a is drawn through the central portion of the grossite primary phase field. It intersects two multiply saturated liquid compositions, both of which project to the same point on CA-An. One of these, point A, is hibonite- and grossite-saturated and the other, less CaAl_4O_7 -rich, point B, is an invariant point, saturated with respect to the three crystalline phases grossite, CaAl_4O_7 , and melilite. It happens that one liquid (point A) is CaAl_4O_7 -rich relative to CA-An and the other, point B, is CaAl_4O_7 -poor (i.e., one above and one below the CA-An line, respectively). If contoured in terms of wt% grossite above or below the CA-An line, one would have positive amounts of grossite component A and one would have negative amounts of grossite component B, but this is an artifact of the selected projection line. If the projection line were CaO-SiO₂, both liquids would be above the projection line (both with positive amounts of grossite component), and if An-CaAl₁₂O₁₉ were used, both liquid compositions would be below the projection line (both with negative amounts of grossite component). The existence of an upper and lower multiple saturation curve in this example from CAS and upper and lower surfaces for comparable examples in CMAS is an endemic feature of projections taken from compositions of incongruently melting phases. While it is possible to construct projections from the compositions of congruently melting phases for which more than one liquid composition projects to the same point, these are not important for CAIs.

Grossite-bearing inclusions are relatively common in CH chondrites and rather rare elsewhere. Figure 3b shows the compositions of grossite-saturated liquidus phase fields projected from CaAl_4O_7 (grossite) onto the plane defined by the end-member compositions CaAl_2O_4 (calcium monoaluminate), MgAl_2O_4 (spinel), and $\text{CaAl}_2\text{Si}_2\text{O}_8$ (anorthite), contoured in wt% CaAl_4O_7 . The depicted fields describe a lower surface of stability for grossite based on data from *Osborn and Gee* (1969), *Gutt and Russell* (1977), *Beckett and Stolper* (1994) and references cited therein, and *de Aza et al.* (1999). There is also an upper stability limit, but this is poorly constrained except in the system CaO-Al₂O₃-SiO₂ (Fig. 3a), which plots along the base of the triangle in Fig. 3b. Here, the maximum wt% of the CaAl_4O_7 component that a bulk composition can have and still have grossite on the liquidus ranges from +70 wt% at the CaAl_2O_4 vertex (lower surface at ~+12 wt% CaAl_4O_7 component) to ~+60 at the calcium monoaluminate-melilite-grossite – liquid invariant point (lower surface at ~-30 wt%) to ~+40 at the 60 wt%

CaAl_2O_4 tic (lower surface at ~-30 wt% CaAl_4O_7 component), after which it drops rapidly to meet the lower surface shown in Fig. 3b. To take a specific example, consider compositions along the CaAl_4O_7 - CaAl_2O_4 join, which plot at the CaAl_2O_4 vertex in Fig. 3b and along the base of the triangle in Fig. 3a. Such compositions will have grossite on the liquidus only for wt% of the CaAl_4O_7 component between ~+12 and +70 wt%. If the bulk composition has less than +12% CaAl_4O_7 component, CaAl_2O_4 or some other phase will be on the liquidus (see, e.g., Fig. 3a) and if there is more than +70 wt% CaAl_4O_7 component, hibonite or corundum will be on the liquidus. The importance of this can be seen from the bulk compositions of grossite-bearing CAIs described by *Weber and Bischoff* (1994), which come in two distinct populations. Bulk compositions of the melilite-rich inclusions (open circles) have -28 to +9 wt% CaAl_4O_7 component; they plot above the lower grossite saturation surface and almost certainly below the upper surface; these inclusions will have grossite on the liquidus, and Fig. 3b can be used to infer the identity of the second crystallizing phase (melilite) and the crystallization sequence provided Ti-contents are sufficiently low. The predicted fractional crystallization sequence for such bulk inclusions would when projected from TiO₂, be grossite → melilite → spinel → either calcium monoaluminate or hibonite, depending on which side of the spinel-melilite thermal divide the residual liquid strikes. CaAl_2O_4 is not observed in these inclusions even though the phase relations suggest that most of them would eventually crystallize CaAl_2O_4 . This may indicate that perovskite is generally relict; the bulk compositions would, if projected from perovskite instead of TiO₂, all plot on the anorthite-rich side of the thermal divide (i.e., some of the Ca in the bulk composition is tied up in perovskite, making the relevant residual liquid compositions less calcic), which in projection, shifts compositions away from the CaAl_2O_4 vertex. The second population of grossite-bearing CAIs (open squares) is characterized by amounts of CaAl_4O_7 component exceeding +70 wt%. Grossite is not the liquidus phase for these bulk compositions (even pure CaAl_4O_7 does not have grossite on the liquidus because the phase melts incongruently), and Fig. 3b cannot be used to infer early portions of the crystallization sequences.

Hibonite is an important phase in many aluminous CAIs, and *Beckett and Stolper* (1994) projected compositions of hibonite-saturated liquid compositions from $\text{CaAl}_{12}\text{O}_{19}$, the nominal end-member composition of hibonite, onto the plane defined by the end-member compositions of gehlenite, anorthite, and spinel (Fig. 4). This tetrahedron shares one face (anorthite-gehlenite-spinel) with the one used by *Stolper* (Fig. 2b), but the fourth vertex (hibonite) lies on the CaO-Al₂O₃ binary rather than MgO-SiO₂ (forsterite). Bulk compositions of some hibonite-rich inclusions and hibonite-glass spherules lie above or close to the hibonite-saturation surface (Fig. 4a), implying that hibonite was a liquidus or near-liquidus phase, but others plot far below the saturation surface. All the glass compositions from hibonite-glass spherules considered by *Beckett and Stolper* (1994) are be-

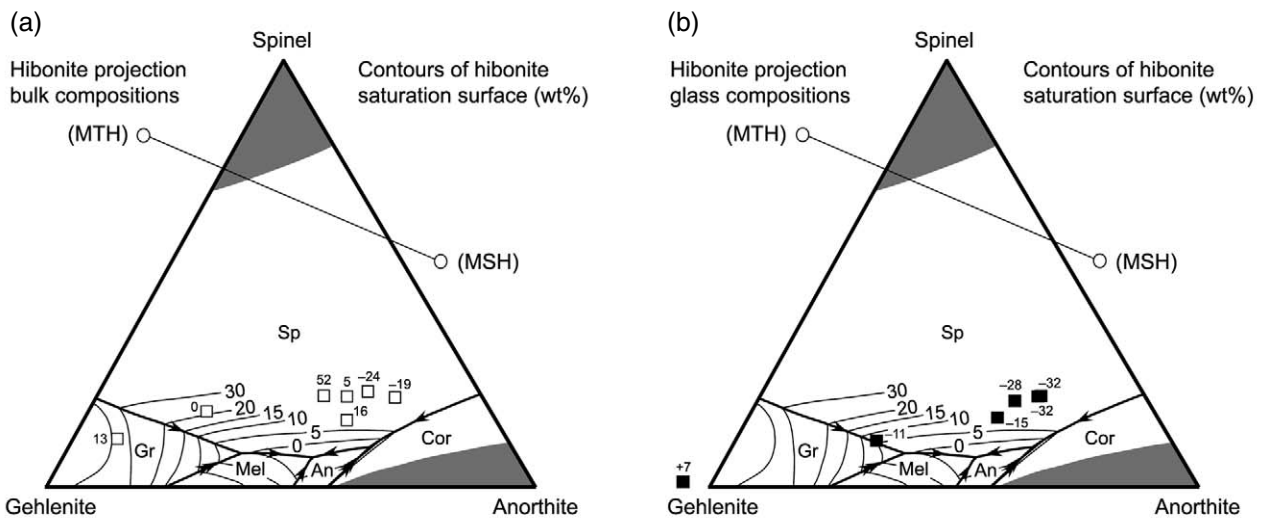


Fig. 4. Projection of hibonite-saturated liquidus surfaces from $\text{CaAl}_{12}\text{O}_{19}$ (hibonite) onto the plane defined by the compositions of gehlenite ($\text{Ca}_2\text{Al}_2\text{SiO}_7$), spinel (MgAl_2O_4), and anorthite ($\text{CaAl}_2\text{Si}_2\text{O}_8$) after *Beckett and Stolper* (1994). The identity of the second saturated crystalline phase is indicated in each field. Shading indicates regions in which there is no stable hibonite-saturated liquid. Projected positions of $\text{CaAl}_{10}\text{MgTiO}_{19}$ (MTH) and $\text{CaAl}_{10}\text{MgTiO}_{19}$ (MSH) are also shown. Gr: grossite. Other abbreviations are as in Fig. 2. **(a)** Bulk compositions of hibonite-rich inclusions. Data from G. J. MacPherson (personal communication, 1991) and *Ireland et al.* (1991). **(b)** Glass compositions in hibonite-bearing inclusions. Data from *Kurat* (1975), *Ireland et al.* (1991), and G. J. MacPherson (personal communication, 1991).

low the saturation surface (Fig. 4b). They took this to imply that hibonite was often relict and, where glass was present, that cooling rates were sufficiently rapid that crystallization of stable phases did not take place. In some cases (*Ireland et al.*, 1991), hibonite and glass are not in isotopic equilibrium, also consistent with the idea that some of the hibonite is relict with respect to the last melting event. A similar theme occurs in a consideration of hibonite crystals in type A inclusions (not shown). Here, bulk compositions plot well below the hibonite saturation surface even though hibonite is texturally early, an apparent inconsistency with the phase relations, which was used as one line of evidence by *MacPherson and Grossman* (1984) that fluffy type As did not crystallize from a melt. The important point is that phase diagrams can be used to help establish inconsistencies with observed phase assemblages and textures and this can lead to the identification of possible relict phases and the effects of processes other than simple equilibrium or fractional crystallization.

3.2.3. Projections for Mg-, Si-rich objects. The often high Fe and Na contents inferred for the melted precursors of ferromagnesian chondrules make CMAS an inappropriate analog system but there are objects whose bulk compositions are intermediate between those of CAIs and ferromagnesian chondrules that are generally referred to as Al-rich chondrules (*Bischoff and Keil*, 1983, 1984; *Sheng et al.*, 1991b; *MacPherson and Huss*, 2005). For some of these, CMAS phase equilibria provide useful constraints, and *Sheng et al.* (1991a) introduced a set of three projections for such inclusions: projection from spinel onto forsterite + silica + anorthite (Fig. 5a); projection from forsterite onto

the plane formed by end-member compositions of spinel, silica, and diopside (Fig. 5b); projection from anorthite onto spinel + silica + diopside (Fig. 5c). The last two diagrams are given in a larger format by *Srinivasan et al.* (2000), taken from *Sheng's* (1992) thesis, and also shown by *MacPherson and Huss* (2005). By selecting the appropriate phase diagram (i.e., the one for which the bulk composition plots above the saturation surface and within the contoured portion of the diagram), *Sheng et al.* (1991a), *Sheng* (1992), *Srinivasan et al.* (2000), and *MacPherson and Huss* (2005) were able to determine crystallization paths for the inclusions they studied. For the most part, once the residual liquid intersected a liquidus phase saturation surface, these authors were able to treat the phase relations shown in the projections in the same way they would have had the projections been true ternary systems. As noted above, this reduction in complexity is one of the great advantages of projections. The apparent simplicity is not always real, however, and there are traps lurking for the unwary within these diagrams. These snares come in two broad classes, those reflecting the properties of projections in CMAS, and those reflecting the consequences of using CMAS for objects containing additional components. Here, we consider projection effects for purely CMAS compositions. In section 3.2.5, we consider problems associated with the addition of non-CMAS components.

One potential problem with projections arises when the phase whose composition is being projected from has a reaction relationship with the liquid. More often than not, this information is left off the figure. Consider Fig. 5a, a projection from MgAl_2O_4 (spinel) onto the plane formed

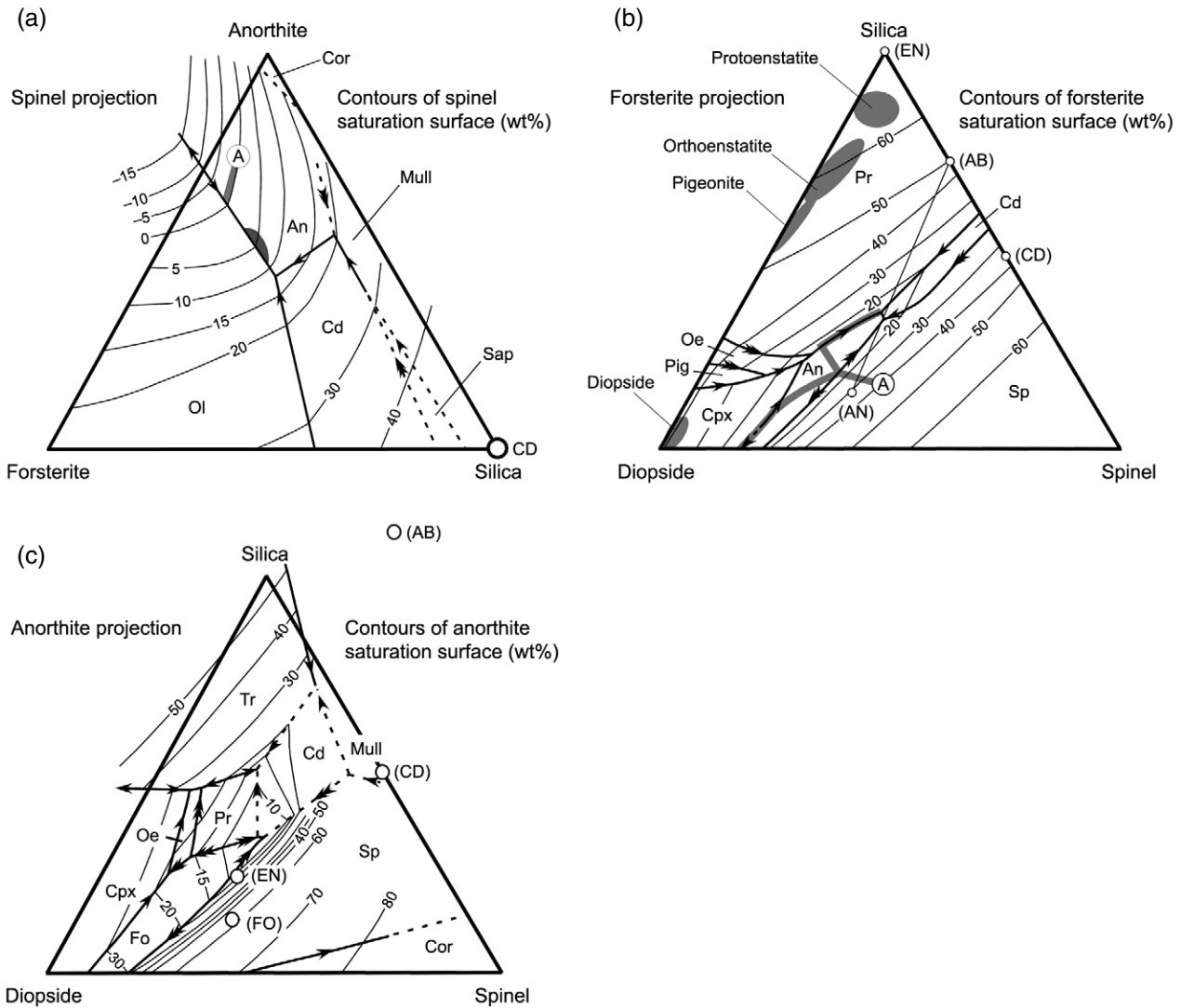


Fig. 5. Projections relevant to the study of Al-rich chondrules after *Sheng et al.* (1991a) and *Sheng* (1992). **(a)** Projection of spinel-saturated liquidus phase fields from the composition of spinel onto the plane defined by the compositions of anorthite, forsterite, and silica. All phase fields are spinel-saturated; the identity of the second crystalline phase is indicated. Contours are in wt% spinel component. The fractional crystallization path for a composition that projects to point A is also shown. The shaded half-ellipse indicates a region on the anorthite + spinel saturation surface where spinel is in a reaction relationship with the liquid. Sap: sapphirine; Cd: cordierite. Abbreviations for other spinel-saturated liquidus phase fields are as in previous figures. CD and the associated open circle refer to the projected position of end member cordierite. **(b)** Projection of olivine-saturated liquidus phase fields from the composition of forsterite onto the plane defined by spinel, silica, and diopside. Note that the panels in this figure appear to have been produced independently and therefore are not consistent with each other in detail. No attempt is made here to map liquid compositions from one panel to the next in order to induce an internal consistency in the phase relations, but the cordierite-spinel-forsterite boundary curve was adjusted to be a reaction curve as it approached the silica-spinel-forsterite join, consistent with behavior expected based on **(a)**. The topology of boundary curves between the anorthite and cordierite fields was also changed from the original diagram to be consistent with expectations based on data of *Longhi* (1987) and *Sheng* (1992) that there is no stable boundary curve in CMAS for forsterite + spinel + protoenstatite + liquid. Oe: orthoenstatite, Pig: pigeonite, and Pr: protoenstatite for spinel-saturated phase fields, and EN (enstatite), AB (albite), and CD (cordierite) for projected positions of end members, which are indicated by open circles. Gray ellipses outline compositions of solids obtained by *Longhi* (1987). Fractional crystallization paths are shown for two bulk compositions, differing only in the presence or absence of Na_2O . The projection is taken from Na_2O so that both bulk compositions plot in the same place, A, in projection. **(c)** Projection of anorthite-saturated liquidus phase fields projected from anorthite onto the plane defined by end-member compositions of spinel, silica, and diopside. Contours are in wt% anorthite component above this plane. Abbreviations include FO for the end member forsterite and Tr to indicate the tridymite-spinel-liquid field, with others as previously defined.

by the compositions of end member forsterite, silica, and anorthite. It shows the compositions of spinel-saturated liquids contoured in wt% spinel component after Sheng et al. (1991a) and Sheng (1992). Let's ignore the fact that Fig. 5a is a projection for a moment (i.e., pretend that spinel is not present and assume that this is a true ternary with "forsterite," "anorthite," and "cordierite" plotting at the vertices). Ignoring any minor solid-solution effects, we would conclude that "anorthite" was the liquidus phase for point A and that fractional crystallization would drive the composition of the residual liquid directly away from the "anorthite" vertex until it reached the "forsterite" + "anorthite" boundary curve. We could determine the nature of the boundary curve by extending a tangent from the curve to the join formed by the instantaneously crystallizing phase assemblage (i.e. the "anorthite"-forsterite join). Since the tangent intersects the join *between* "anorthite" and "forsterite," the composition of the instantaneously crystallizing phase assemblage is described by positive amounts of both "anorthite" and "forsterite"; in our imaginary ternary, this means the boundary curve is a subtraction curve and that "anorthite" and "forsterite" co-crystallize along it. The composition of the residual liquid moves with decreasing temperature, or equivalently, with increasing degree of crystallization along the curve away from the "anorthite"-forsterite join until it reaches the "cordierite"-anorthite-forsterite invariant point. Since the invariant point lies inside the composition triangle defined by "anorthite" + "forsterite" + "cordierite," the liquid composition can be described in terms of positive amounts of these three phases and the liquid would therefore crystallize "anorthite," "forsterite," and "cordierite" in a constant ratio until it was exhausted. Sounds simple. Now, let's consider fractional crystallization for a liquid plotting at point A when Fig. 5a is treated as the spinel projection it actually is. To be specific, let A have 3 wt% spinel component, which would be typical of some Al-rich chondrules studied by Sheng and co-workers (see also Wark, 1987). Since point A plots on top of the 0 wt% spinel contour, spinel is the liquidus phase and Fig. 5a is a suitable projection for determining crystallization sequences. If this liquid is cooled from above its liquidus, Fig. 5a predicts that spinel crystallizes first and the liquid composition is driven directly away from spinel until it strikes the saturation surface. While crystallizing spinel alone, the residual liquid continues to plot in projection at point A because it is projected from the composition of the instantaneously crystallizing phase assemblage (i.e., MgAl₂O₄ spinel). Once the liquid encounters the spinel-saturated liquidus surface, anorthite becomes a stable phase. At this point, we can ask what happens if anorthite is allowed to crystallize by using the same approach as in the imaginary ternary exercise but taking into account that the projection describes a surface: Take a tangent to the saturation surface in the direction of the join describing compositions of the two solids spinel and anorthite. Since all compositions are projected from spinel, the composition of this

instantaneously crystallizing phase assemblage projects to the anorthite vertex. From the contours, we can see qualitatively that the tangent's intersection with this join will occur *between* anorthite, which plots at 0 wt% spinel component, and spinel, which has 100% spinel component. So, anorthite and spinel co-crystallize and the projected liquid composition moves along the saturation surface away (in projection) from anorthite until it strikes the anorthite-forsterite-spinel boundary curve. This is just the sequence expected based on a simple ternary approach ignoring spinel. Now, Fig. 5a shows a single arrow on the boundary curve, which is associated in true ternaries with a subtraction curve. It might therefore be tempting to simply assume that anorthite, olivine, and spinel co-crystallize and that the liquid composition evolves along this curve until it reaches the cordierite-anorthite-forsterite-spinel invariant point, just as expected from a pure ternary approach. We might then conclude that the phase diagram was predicting the presence of cordierite and that no pyroxene of any sort should be expected. Since the inclusions in question generally have little or no cordierite but lots of low-Ca pyroxene (Sheng et al., 1991b), a serious discrepancy would be "discovered" and a speculative discussion of kinetics or relict phases might ensue based on what turns out to be a bad assumption. In general, projections in use for Al-rich objects from meteorites do not indicate where there are reaction relationships involving the projected phase and this includes Fig. 5a. The single arrow on the forsterite-anorthite-spinel boundary curve is saying that neither anorthite nor forsterite is in a reaction relationship with the liquid but it says nothing about whether or not spinel is. The true three-dimensional nature of this boundary curve with respect to spinel can be determined by taking a tangent to the curve, remembering that this is now a space curve, back to the composition plane formed by the three phases anorthite, forsterite, and spinel. This point will plot in projection along the anorthite-forsterite join, but a look at the contours in Fig. 5a shows that the boundary curve slopes down enough to make the tangent intersect this plane outside the triangle formed by the crystallizing phase assemblage, to the spinel-poor side of anorthite-forsterite. This means that the instantaneously crystallizing phase assemblage requires negative amounts of spinel (i.e., spinel is in a reaction relationship with the liquid). For perfect fractional crystallization in which all solids are immediately removed from contact with the liquid, a liquid evolving from point A will leave the spinel-saturation surface once it strikes the anorthite-forsterite-spinel boundary curve, whereupon Fig. 5a is no longer pertinent. Based on Fig. 5a, Al-rich chondrules whose compositions lead them to the anorthite-forsterite-spinel boundary curve will have spinel in a reaction relationship. For such Al-rich chondrules, one should therefore be looking for evidence of resorption or armoring of spinel where present, as is observed in these Al-rich chondrules. Another phase diagram (e.g., Fig. 5b) is needed to help follow later stages of fractional crystallization. The prediction, based on a pure ternary

approach to Fig. 5a, that cordierite crystallization should follow olivine but that pyroxene crystallization should not be a mirage.

Finally, we note as an aside that the nature of a boundary curve can usually be determined quantitatively by taking a tangent to the boundary curve, if an equation is given for it, or, much more likely, by writing four mass balance equations relating compositions of the three crystalline phases plus a liquid composition along the boundary curve to the composition of a nearby down-temperature liquid. For CaO, this can be represented by

$$n_{\text{CaO}}^{\text{Xl}\#1} n_{\text{Xl}\#1} + n_{\text{CaO}}^{\text{Xl}\#2} n_{\text{Xl}\#2} + n_{\text{CaO}}^{\text{Xl}\#3} n_{\text{Xl}\#3} + n_{\text{CaO}}^{\text{Liq}\#1} n_{\text{Liq}\#1} = n_{\text{CaO}}^{\text{Liq}\#2}$$

where n_{CaO}^j is the number of moles of CaO in phase j , n_j is the number of moles of phase j , and $\text{xl}\#i$ refers to crystalline phase i . Similar equations can be written for each of the oxides, MgO, Al₂O₃, and SiO₂, and the resulting set of four linear equations in four unknowns solved. One can also use the components of the figure on a molar basis rather than converting to end-member oxides. In either case, the mass balance defines relative amounts of phases produced or consumed. If positive amounts of all the crystalline phases are required to produce the down-temperature liquid, the boundary curve is a subtraction curve. Negative amounts indicate a reaction curve and the signs point the way to which phase(s) has a reaction relationship with the liquid.

3.2.4. Going for a more global view. Projections described in the previous two subsections were designed primarily to portray the phase relations for composition volumes relevant to one or a few groups of CAIs or related objects. If one attempts to plot compositions of CAIs from other groups or objects that might be related to CAIs on these diagrams, they often project to great distances from the composition triangles used to define the projection planes. This makes it difficult to see possible relationships among the different groups. *MacPherson and Huss* (2005) dealt with this problem by projecting spinel-saturated liquidus phase fields from MgAl₂O₄ onto the plane defined by Mg₂SiO₄, Al₂O₃, and Ca₂SiO₄ (Fig. 6a). The ternary used in Stolper's projection, in which compositions are also projected from spinel, is outlined within Fig. 6a by joining the points GE (gehlenite), AN (anorthite), and Mg₂SiO₄ (FO; forsterite). Figure 5a (AN-FO-SIL) can also be seen as a face of the hibonite-anorthite-gehlenite-spinel tetrahedron used by *Beckett and Stolper* (1994).

Figure 6a is after the phase diagram presented by *MacPherson and Huss* (2005), differing only in handling of phase fields plotting toward the base of the triangle, which are not important for the interpretation of phase equilibria relevant to CAIs or Al-rich chondrules. The merwinite (MER; Ca₃MgSi₂O₈) - melilite (+ spinel) and merwinite - periclase (+ spinel) boundary curves are reasonably well-determined (*Prince*, 1951; *Osborn et al.*, 1954; *Gutt*, 1964, 1968; *Osborn and Gee*, 1969). Compositions of bredigite

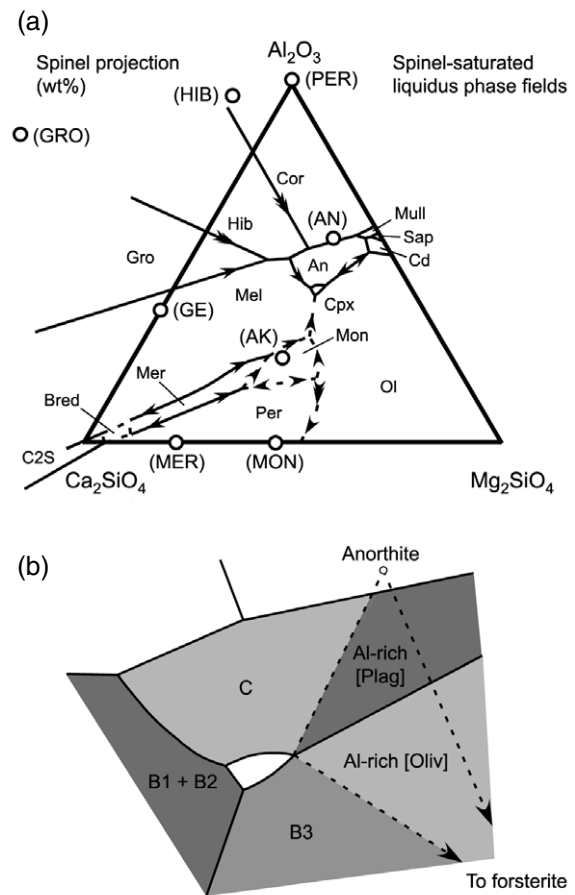


Fig. 6. (a) Projection of spinel-saturated liquidus phase fields from MgAl₂O₄ onto the plane defined by Mg₂SiO₄, Al₂O₃, and Ca₂SiO₄, modified after *MacPherson and Huss* (2005). In each field, a liquid coexists with spinel and the crystalline phase indicated in or near the field. Projected positions of end-member compositions of crystalline phases are indicated in caps enclosed in parentheses. Bred: bredigite (Ca₅MgSi₃O₁₂), C2S: Ca₂SiO₄, and Per: periclase for phases; MER: merwinite (Ca₃MgSi₂O₈) and PER: periclase (MgO) for end members. Other abbreviations are as defined in previous figures. See text for data sources. (b) A schematic portion of (a) centered on the clinopyroxene + spinel + liquid field. Solid curves are boundary curves. Dashed lines are drawn between the end-member compositions of anorthite and forsterite or between an end-member composition and an invariant point.

(Ca₅MgSi₃O₁₂)-saturated (+ spinel) liquids are not available but a field is shown truncating the merwinite field in Fig. 6a to be consistent with experimental work of *Biggar* (1971); we neglect a likely stable spinel-saturated liquidus field for the compound Ca₆MgAl₈O₂₁ (*Biggar*, 1971). Phase relations involving monticellite + spinel are not well constrained, and the positioning of the olivine - melilite (+ spinel) boundary curve is also surprisingly uncertain. Placement of the latter curve in *Stolper* (1982) was based on the intersection of three dashed lines in a figure from *Schairer and Yoder*

(1969). Taking all available experimental data at face value, the periclase-olivine (+ spinel) boundary curve extends past the periclase + monticellite + olivine (+ spinel) invariant point well into the olivine field shown in Fig. 6a but this is inconsistent with data for olivine-, spinel-saturated liquids that would end up on the wrong side of the boundary curve (e.g., DeVries and Osborn, 1957; Gutt, 1964; Osborn and Gee, 1969). We assumed in constructing Fig. 6a that the stable periclase + olivine (+ spinel) boundary curve is truncated by the monticellite field and that extensions of the boundary curve into the olivine field are metastable, perhaps reflecting the metastable persistence of periclase in experimental run products. An alternative extension of the monticellite field toward Mg_2SiO_4 - Ca_2SiO_4 seems unlikely given the large collection of experimentally produced spinel + olivine- (no periclase)-saturated liquids in this region and the well-defined position of the periclase + olivine + liquid field in the MAS system, which plots in projection on an extension of Al_2O_3 - MgAl_2O_4 , well below the triangle shown in Fig. 6a. The precise position and extent of the monticellite + spinel + liquid field is highly uncertain, but since igneous monticellite and periclase are not found in CAIs or related objects, this is not a significant problem for the present purposes. Clarification of the phase relations in this portion of the phase diagram would probably require additional experimentation.

Figure 6b, modified after MacPherson and Huss (2005), shows a portion of the spinel-saturated phase equilibria displayed in Fig. 6a (see also Fig. 2b) with the regions where bulk compositions of specific types of objects plot indicated by shaded fields. Consider bulk compositions that project to either the Al-rich [Plag] or Al-rich [Oliv] shaded regions; upon fractional crystallization, residual liquids evolve to the olivine-anorthite + spinel boundary curve. Since spinel is in a reaction relationship along this curve, the liquids leave the spinel saturation surface and melilite does not appear during crystallization. These objects will become Al-rich inclusions and not CAIs. This fundamental distinction in phase assemblage wrought by the phase relations is the basis for the MacPherson and Huss (2005) classification scheme. The distinction between Al-rich [Plag] and Al-rich [Oliv] is also derived from the phase relations. Bulk compositions of Al-rich [Plag] chondrules project to the spinel + anorthite + liquid saturation surface. Anorthite will precede olivine in the crystallization sequence for these objects. Bulk compositions of Al-rich [Oliv] chondrules project to the spinel + olivine + liquid saturation surface. Olivine precedes anorthite in the crystallization sequence. These behaviors contrast fundamentally with those expected for the shaded regions shown for type B1/B2, B3, and C inclusions. In each, fractional crystallization leads residual liquid compositions to the melilite stability field so that melilite is generally expected to be part of the phase assemblage for these objects. The first silicate, or in some cases, first crystallizing phase will be melilite in the B1 + B2 field, olivine for B3, and anorthite for C. Thus, the classification

of many CAIs and Al-rich chondrules is a direct reflection of the phase relations, both in terms of the presence or absence of phases and in terms of order of crystallization.

A major advantage of large-scale phase diagrams like Fig. 6a is that suites of objects ranging from the most aluminous CAIs to the most magnesian of amoeboid olivine aggregates (AOAs), Al-rich chondrules, and even ferromagnesian chondrules can be plotted on the same diagram (MacPherson and Huss, 2000, 2005; Krot et al., 2001; MacPherson et al., 2004) (see also Fig. 1). The principle disadvantages of the MacPherson/Huss diagram are consequences of the same features that make the diagram so useful for seeing how broad variations in composition play out for multiple types of objects. Although it is possible to plot virtually any bulk CAI composition on Fig. 6a, the phase relations refer only to spinel-saturated liquids. While spinel is the liquidus phase for many CAIs, melilite is on the liquidus for type As, grossite or hibonite for most highly aluminous CAIs, olivine for some B3s, and olivine or plagioclase for many if not most Al-rich chondrules. For most inclusions, it should be possible to use a version of the MacPherson and Huss (2005) phase diagram, in which the spinel saturation surface has been contoured in terms of wt% MgAl_2O_4 component, to determine if the phase relations are applicable, but smaller-scale diagrams (e.g., sections 3.2.1–3.2.3) may be necessary.

3.2.5. When to get nervous: Nonquaternary components. All CAIs and all Al-rich chondrules contain non-CMAS components and, if too much of one or more is present during crystallization, the phase relations depicted in a CMAS projection may be so poorly connected to the actual system defined by the object as to be useless or, even worse, misleading. The bounds beyond which the use of CMAS becomes problematic have not been studied rigorously and we provide only general guidance here. The problems associated with extra components fall into two basic categories:

1. CMAS-based phase relations are adequate, at least for determining crystallization sequences, but incorporation of non-CMAS components into a solid solution affects how one interprets the diagram.

One problem with non-CMAS components is that, if they are soluble in a crystalline phase, thermal divides involving that phase will shift even if the boundary curves and saturation surfaces hardly budge, and this can lead to fundamental changes in crystallization sequences. MacPherson and Huss (2005) give an example of this for an Al-rich chondrule, 4128-3-2 from Semarkona (Plate 11g), and point A in Fig. 5b shows a similar composition. Let's presume first that point A is in CMAS and plots above the olivine saturation surface. Fractional crystallization of the bulk will drive the composition of residual liquids away from the composition of forsterite until the forsterite-spinel saturation surface is intersected, the compositions of the residual liquids all projecting to point A, neglecting small amounts of Ca_2SiO_4 in the olivine. Spinel now joins

the crystallizing phase assemblage and the residual liquid moves away in projection from the spinel vertex until the boundary curve is encountered. Spinel is in a reaction relationship with the liquid along this boundary curve, so the residual liquid strikes out across the anorthite-forsterite saturation surface directly away from the composition of end member anorthite until it hits the forsterite + anorthite + protoenstatite boundary curve, which it follows to the forsterite + anorthite + protoenstatite + orthoenstatite invariant point where protoenstatite is in a reaction relationship and the residual liquid leaves the saturation surface. So, the CMAS phase diagram makes a clear prediction that the phase assemblage produced from composition A in Fig. 5b will have protoenstatite but little or no calcic pyroxene. The problem for *MacPherson and Huss* (2005) was that Al-rich chondrule 4128-3-2 had lots of calcic pyroxene and no low-Ca pyroxene. Now, MacPherson and Huss could have danced around with *ad hoc* errors in the bulk composition, suggested that something odd happened to the chondrule, or, perhaps, argued that Na, which was present during melting based on compositions of igneous plagioclase, dramatically stabilized diopside relative to protoenstatite. *MacPherson and Huss* (2005), however, pointed to a simple alternative. They noted that plagioclase in their chondrule is somewhat sodic ($\sim\text{An}_{80}$). Such a feldspar composition will not project to the composition of anorthite in Fig. 5b, instead plotting along the anorthite-albite join. How does this affect the predicted crystallization sequence? If enough Na is present, then the CMAS phase diagram is simply inapplicable, but let's assume that the amount of Na is insufficient to substantially affect the positions of boundary curves as given by CMAS phase equilibria. Residual liquids produced by fractional crystallization of A will follow the same path in projection as they would for CMAS down to the anorthite + forsterite + spinel boundary curve provided they are projected from Na_2O . Once plagioclase begins to crystallize, however, the residual liquid is driven away from the composition of the Na-bearing feldspar, whose composition lies further up the anorthite-albite join than does end member anorthite. The residual liquid is still driven across the plagioclase + forsterite saturation surface but the direction is altered relative to expectations based on CMAS and it is the diopside + plagioclase + forsterite boundary curve that is intersected, not protoenstatite + plagioclase + forsterite (Fig. 5b). Moreover, the thermal divide along this curve, which is the intersection of the plane defined by the compositions of coexisting forsterite, plagioclase, and diopside with the boundary curve, migrates toward albite as the plagioclase incorporates Na. Having reached this boundary curve, further crystallization drives residual liquids away from the low-Ca pyroxene fields, consistent with the observed phase assemblage in the chondrule.

Unexpected projection effects can also arise when projecting liquid compositions from the composition of a crystalline phase that contains significant amounts of a non-CMAS component because ignoring an oxide in a bulk composition is equivalent to projecting from that oxide. Suppose, for example, in Fig. 5b, that liquid A is in CMAS

and above the olivine saturation surface. Ignoring minor Ca_2SiO_4 , the bulk composition and residual liquid compositions after fractional or equilibrium crystallization of olivine plot in the same place (i.e., at A) until spinel joins the crystallization sequence. If the initial liquid composition contains significant amounts of FeO, however, olivine will incorporate some of this as fayalite (Fe_2SiO_4) during crystallization. Since fayalite plots at the silica vertex when projected from Mg_2SiO_4 (forsterite) and FeO, crystallization of the Fe-bearing olivine drives the residual liquid composition in projection directly away from the silica vertex. How far depends on how much olivine crystallization is involved and how Fe-rich the olivine, but it is not difficult to conceive of circumstances under which predicted crystallization sequences would be affected. Similar effects can arise during crystallization of Ti-bearing hibonite (Fig. 4), residual liquid compositions moving away from MTH, and of Na-bearing plagioclase in Fig. 5c, residual liquids moving away from the composition of plagioclase, which plots along the join AN-AB.

2. If too much of a non-CMAS oxide is added to a composition, finessing the phase relations as described in the preceding paragraphs fail, either because the relative stabilities of solid phases change, leading to shifts in saturation surfaces and boundary curves, or the topology of the phase diagram changes because a new CMAS or non-CMAS phase is stabilized or an old one disappears. Even when a projection looks much the same after the addition of some non-CMAS oxide, temperatures on the saturation surfaces may change significantly. Here, we supply a few semi-quantitative constraints with respect to the oxides of Na, Ti, and Fe. We ignore the effects of other oxides, sulfide-rich liquids, and the metallic phase, the first because they are generally present in very low concentrations, and the latter two because they are immiscible with negligible solubility in the coexisting silicate liquids under the reducing conditions of interest here.

Small amounts (<1 wt%) of Na_2O have little effect on melilite + spinel equilibria according to *Beckett and Stolper* (2000), and *Sheng* (1992) showed that 4 wt% Na_2O had a only modest effect on the anorthite-, spinel-, forsterite-saturated phase boundary shown in Fig. 5b. On the other hand, *Kushiro* (1975) noted that the stability field of forsterite + liquid in the MgO-SiO_2 system expands relative to that of enstatite + liquid as Na is added. Also, *Longhi and Pan* (1988), *Pan and Longhi* (1990), and *Sheng* (1992) found that increasing Na generally decreased the liquidus temperature relative to expectations based on CMAS, suppressed plagioclase crystallization, expanded the spinel + forsterite field relative to forsterite + cordierite, and reduced the spinel + forsterite field relative to those of diopside + forsterite and melilite + forsterite, though usually several mol% Na_2O was required to make the changes obvious.

Changes in the relative stabilities of crystalline phases in liquids can be quantified for liquids relevant to CAIs and Al-rich chondrules through a consideration of relative affinities (e.g., *Prigogine and Defay*, 1954). When a liquid is in equilibrium with a solid phase, the difference in chemi-

cal potential relative to a common standard state, or affinity, is zero. For example, for olivine coexisting with liquid, we can define the affinity as

$$A_{\text{fo-liq}} = \mu_{\text{Mg}_2\text{SiO}_4}^{\text{ol}} - 2\mu_{\text{MgO}}^{\text{liq}} - \mu_{\text{SiO}_2}^{\text{liq}}$$

where μ_i^j is the chemical potential of component i in phase j . Similar expressions can be written for other crystalline phases. Now, suppose in some experiment that two crystalline phases are in equilibrium with the same Na-bearing liquid. The affinity for each crystalline phase relative to the liquid is zero since it is in equilibrium with the Na-bearing liquid. If the chemical potentials of components in the liquid are calculated based on CMAS, the affinities will in general be different from zero and, more to the point, different from each other. These differences are a measure of the relative stabilization or destabilization of the crystalline phases as Na is added to the system. Figure 7 shows the affinity for forsterite relative to other phases calculated for Na-bearing liquids using the thermodynamic model of *Berman* (1983), which is described in section 3.3.1. Each point was derived either from a glass analysis taken from an experimental run product or through digitization of a phase diagram. A positive value indicates that forsterite is stabilized relative to the second crystalline phase; a negative value implies relative destabilization of forsterite. Based on reconnaissance calculations using *Berman's* (1983) model, an affinity difference exceeding several kJ/mole generates shifts in saturation surfaces severe enough to render suspect a graphical determination of crystallization paths based on CMAS figures. From Fig. 7, forsterite is stabilized relative to spinel and protoenstatite and destabilized relative to diopside. At constant $X_{\text{Al}_2\text{O}_3}^{\text{liq}}/X_{\text{SiO}_2}^{\text{liq}}$ in the liquid, the effect of additional Na on the relative stabilities is muted over some range in Na but, with further additions of Na, the stability of one phase is strongly enhanced over the other. In general, values of $X_{\text{Na}_2\text{O}}^{\text{liq}}$, the mole fraction of Na_2O in the liquid, beyond which large changes in relative affinity occur, increase with increasing Al/Si in the melt. The relevant ranges in $X_{\text{Al}_2\text{O}_3}^{\text{liq}}/X_{\text{SiO}_2}^{\text{liq}}$ are ~0.25–0.40 for type B and C CAIs and ~0.15–0.30 for Fe-poor, Al-rich chondrules, leading to strong differences in affinity for $X_{\text{Na}_2\text{O}}^{\text{liq}}$ above ~0.05 mol% Na_2O except for spinel + forsterite in low Al/Si liquids relevant to some Al-rich chondrules, for which limiting the use of CMAS projections to liquids with $X_{\text{Na}_2\text{O}}^{\text{liq}} < 0.03$ is a safer bet. Similar diagrams for diopside-anorthite, forsterite-anorthite, and spinel-anorthite based on data of *Biggar* (1984), *Bowen* (1915), *Libourel* (1999), *Pan and Longhi* (1990), *Schairer and Morimoto* (1959), *Schairer and Yoder* (1960, 1961), *Schairer et al.* (1967), and *Soulard et al.* (1992) are consistent with the idea that forsterite and diopside are stabilized relative to plagioclase as Na is added to CMAS liquids independent of Al/Si, both relative affinities being approximately proportional to $(X_{\text{Na}_2\text{O}}^{\text{liq}})^2$ at least for $X_{\text{Na}_2\text{O}}^{\text{liq}} < \sim 0.08$.

We noted above that the addition of several wt% TiO_2 to liquids within some of the subsystems of CMAS led to variably reduced appearance temperatures for crystalline phases but that crystallization sequences were the same as in the

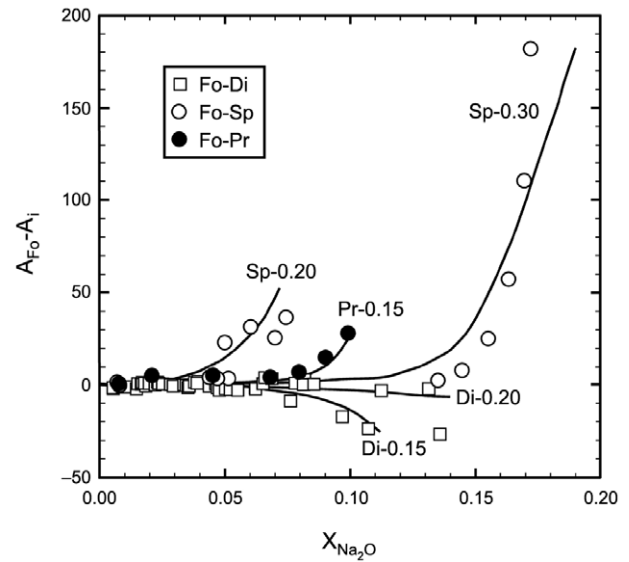


Fig. 7. The effect of Na_2O addition to CMAS liquids on the relative stabilities of liquidus phases. Each point represents a CMAS + Na_2O liquid in equilibrium with two or more crystalline phases but with affinities calculated ignoring Na (i.e., liquid compositions normalized to CMAS). Affinities of diopside, protoenstatite, and spinel relative to the affinity of forsterite are shown. Values were calculated using the model of *Berman* (1983) for CMAS liquids and end-member crystalline phases. The curves are labeled by phase (Di: diopside; Pr: protoenstatite, Sp: spinel) and molar $\text{Al}_2\text{O}_3/\text{SiO}_2$ in the liquid. The curves are visual aids only but are consistent with the data in that liquids with higher $\text{Al}_2\text{O}_3/\text{SiO}_2$ than the curves (± 0.01) plot at higher values of Na_2O . Data are from *Biggar* (1984), *Bowen* (1915), *Libourel* (1999), *Onuma and Yagi* (1967), *Pan and Longhi* (1989, 1990), *Schairer* (1957), *Schairer and Morimoto* (1959), *Schairer and Yoder* (1960, 1961), *Schairer et al.* (1967), *Soulard et al.* (1992), and *Yagi and Onuma* (1969).

Ti-free system to a good approximation provided perovskite or some other Ti-rich phase was not stabilized. *Stolper* (1982) found for compositions relevant to type B inclusions, and *Beckett and Stolper* (1994) for hibonite-rich inclusions, that the addition of a few wt% TiO_2 had no significant effect on predicted crystallization sequences. *Longhi and Pan* (1988) were also unable to discern a TiO_2 effect in compositionally more complex melts with <5 wt% TiO_2 but they found significant differences for liquids with more than ~5 wt% TiO_2 . Thus, the danger point for using CMAS phase relations to interpret basic crystallization sequences for CMAST liquids appears to be several wt% TiO_2 for most liquids and, given the low bulk concentrations for this oxide in most CAIs and Al-rich chondrules, TiO_2 generally becomes problematic only for late-stage crystallization.

In CAIs, FeO contents during melting were negligible but the same is not true for many Al-rich chondrules, and here the issue of how much to trust a CMAS analysis must be confronted. While the topology of CMAS phase diagrams relevant to Al-rich chondrules appear to be largely unaffected except at fairly high concentrations of FeO (*Longhi and Pan*, 1988; *Shi and Libourel*, 1991), there are substan-

tial shifts in the positions of phase boundaries even with modest additions. *Sheng* (1992) (see also *MacPherson and Huss*, 2005) showed that the addition of 6 wt% FeO shifted the forsterite + anorthite + spinel and forsterite + anorthite + protoenstatite boundary curves shown in Fig. 5b substantially toward the silica vertex, largely a consequence of destabilization of protoenstatite. This led *MacPherson and Huss* (2005) to make use of a set of diagrams produced by *Longhi and Pan* (1988) and calculations using the program MELTS (*Ghiorso and Sack*, 1995) to constrain crystallization paths in Al-rich inclusions whenever FeO contents rose above ~3 wt%. *Longhi and Pan* (1988) documented shifts in the spinel + forsterite field and for olivine saturated liquidus fields with protopyroxene, orthopyroxene, pigeonite, and clinopyroxene with changing FeO contents in the liquid or, equivalently, in the olivine. At some point a judgment call needs to be made, but it seems unlikely that usage of CMAS phase diagrams is justified for determining crystallization sequences of FeO-bearing liquid compositions when there is more than 2–3 wt% FeO in the liquid.

3.3. Calculation of Phase Relations in the System CaO-MgO-Al₂O₃-SiO₂ Using Thermodynamic Models

In the previous section, we considered phase relations pertinent to CAIs and related objects based on graphical representations of experimentally determined phase equilibria. This approach is very useful if bulk compositions can be described in terms of quaternary or lower variance systems and if there is enough data in the composition region of interest to allow confident construction of an appropriate phase diagram. If the database is weak, locations of phase boundaries may become little more than intuitive guesses. If more than four components are required, projections carefully tailored to minimize distortions caused by additional components, multiple projections, or empirical fits to boundary curves are usually needed to capture the essence of the phase equilibria (*Walker et al.*, 1979; *Longhi and Pan*, 1988; *Bartels and Grove*, 1991; *Shi*, 1992). An alternative is to determine the thermodynamic properties of all phases in a system and calculate stable phase assemblages through the thermodynamic requirement that a stable phase assemblage have the minimum free energy. In principle, such an approach can be applied to systems with any number of components. Suppose, for example, that we know the composition of a CMAS liquid in equilibrium with anorthite at some temperature and that the thermodynamic model for the liquid uses end-member solid oxides as components. From the reaction $\text{CaO}_{(\text{liq})} + \text{Al}_2\text{O}_3_{(\text{liq})} + 2\text{SiO}_2_{(\text{liq})} = \text{CaAl}_2\text{Si}_2\text{O}_8(\text{plagioclase})$, the free energy of reaction can be expressed as

$$G_{\rightarrow} = 0 = G_{\rightarrow}^{\circ} + RT \ln \left(\frac{a_{\text{CaAl}_2\text{Si}_2\text{O}_8}^{\text{plagioclase}}}{a_{\text{CaO}}^{\text{liq}} a_{\text{Al}_2\text{O}_3}^{\text{liq}} (a_{\text{SiO}_2}^{\text{liq}})^2} \right) \quad (1)$$

where G_{\rightarrow}° refers to the standard state free energy of reaction (all components in their standard state), a_i^j to the activ-

ity of component i in phase j , R to the gas constant, and T to temperature in degrees Kelvin. If a different set of end-member components is used to describe the liquid composition, a different reaction will result but the number of constraints arising from a given crystal-liquid pair remains the same. If a crystalline phase is a solid solution, additional equations analogous to equation (1) can be written for each component in the solid and if a liquid is multiply saturated, each phase generates one or more equations similar to equation (1).

Making use of equation (1) requires an expression for G_{\rightarrow}° and each of the activities (*Anderson and Crerar*, 1993). The usual approach is to define standard-state free energies of formation and activity-composition relationships for the solid phases primarily from solid state thermodynamic data, while phase equilibria and constraints of the type represented by equation (1) are used to determine the thermodynamic mixing properties of the liquid (*Berman*, 1983; *Ghiorso and Sack*, 1995). The basic idea is to then fit expressions for the activity of each component in the liquid as functions of liquid composition and temperature through differentiation of an equation for the excess free energy, a collection of equations analogous to equation (1), and information concerning the thermodynamic properties of the solids, using multiple regression or linear programming (e.g., *Berman and Brown*, 1984) techniques. Once an equation of state for the liquid is defined in this manner, equilibrium phase assemblages can be obtained through free energy minimization for a bulk composition (e.g., *Ghiorso*, 1994) and, therefore, a phase diagram can be constructed even in regions of composition space for which there are no experimental data. Moreover, values for activities of components in the liquid can be specified for any liquid composition at any temperature.

An internally consistent model for silicate liquids will always give an answer to the question of what the activity of a component in the liquid is according to the model, but there are a number of reasons beyond quality of input data for why such predictions may be inaccurate. For example, statements of equilibrium within a given liquidus phase field constrain only relative values of activities for certain components in the liquid. For the anorthite example given above, there is one constraint from the presence of anorthite (equation (1)) and one from the Gibbs-Duhem equation but, with four components, specific values are not determined for any component unless $\text{CaAl}_2\text{Si}_2\text{O}_8$ happens to be selected as one of them. In general, large systematic errors can be accommodated while obeying all available phase equilibria constraints. *Chamberlin et al.* (1994), for example, found experimentally determined MgO and Al₂O₃ activities in CAI-like liquids, most of them spinel-saturated, to be systematically lower than predicted by *Berman's* (1983) model and silica activities systematically higher. A second difficulty with using solution models to predict the thermodynamic properties of silicate liquids is that most of the constraints on liquid properties are based on liquidus data, which is not very good for separating out contributions to the free energy of reaction due to differences in temperature from those due

to differences in liquid composition. Thus, the quality of activity predictions can be expected to decline away from the liquidus, perhaps precipitously. Condensation and/or volatilization calculations, which involve equilibrium between a vapor and a liquid, are often performed for conditions in which no crystalline phases are present (i.e., above the liquidus). While it is hoped that a combination of data for multiple phases in various portions of the system used to calibrate the model adequately constrains activities in all part of the system at all temperatures of interest, there is no guarantee that this is a sound assumption. In the following two subsections, we consider some specific models for the thermodynamic properties of CMAS liquids.

3.3.1. Berman's model. The most frequently used model for CAIs was developed by *Berman* (1983). It has been used to investigate the stability of silicate liquids in nebular environments (*Yoneda and Grossman, 1995; Ebel and Grossman, 2000*); establish activities of major-element oxides in trace-element partitioning reactions (*Beckett et al., 1990, 2000; Beckett and Stolper, 1994, 2000*); constrain the thermodynamic properties of UNK, an unnamed Ti-bearing phase (*Paque et al., 1994*); and predict the thermodynamic contributions to diffusive properties and volatilization behavior of CAI-like liquids (*Richter et al., 2002*). The principle advantages of Berman's model are that it was calibrated for the entire CMAS system using a considerable amount of phase-equilibrium data for quaternary liquids, and it is generally available. Disadvantages, in addition to general problems discussed in the previous paragraph, include the fact that solid solutions are not explicitly modeled; the solution model for the liquid is based on end-member oxides, which means that the entropy of mixing is very poorly represented; and, as noted by *Hashimoto* (1991), the thermodynamic properties of the solids were allowed to vary in a way that almost certainly led to portions of the free energy function for the liquid being distributed among the various solids. Also, according to *Barron* (1985), *Berman and Brown's* (1984) model for CAS liquids is inconsistent with liquid immiscibility constraints (i.e., the model for the liquid is flawed), and this criticism can also be leveled at *Berman's* (1983) model for CMAS. In spite of its faults, Berman's model remains a useful tool.

3.3.2. Other models. Although *Berman's* (1983) model for CMAS liquids has dominated usage in the CAI literature, perhaps largely through inertia, alternative formulations are becoming available. The IRSID model of *Gaye and Welfringer* (1984) uses a cell model to describe interactions within the liquid. They calculated phase diagrams for CAS and the 30 wt% Al₂O₃ plane of CMAS, and showed good agreement with experimentally determined silica activities in CAS. *Ban-ya* (1993) used a regular solution model with oxide end members for multicomponent liquids in describing alloy-slag equilibria. In principle, the model can be used for CMAS liquids, but agreement between predicted and experimentally determined (*Rein and Chipman, 1963, 1965; Chamberlin et al., 1994; Liang et al., 1997*) activities in CAS and CMAS is generally poor. *Björkwall et al.* (2001) used an ionic model based on binary

interactions but, as with *Ban-ya's* (1993) model, agreement with experimentally determined activities of oxide components is not very good.

Most efforts to model the thermodynamic properties of CMAS liquids involve the selection of a set of end members for the liquid. *Hallstedt et al.* (1994) chose an ionic model and were apparently able to reproduce phase equilibria in CAS but at the cost of using a large number of arbitrary ternary parameters, suggesting that simple ionic models are not viable over large portions of CMAS. The proprietary FactSage package (*Bale et al., 2002*), developed by Pelton and coworkers, uses a quasichemical model for the liquid (e.g., *Pelton and Blander, 1984; Pelton et al., 2000*). While a full optimization is available for CAS (also CAS + FeO_x), other ternaries in CMAS have either not been evaluated at all or are only partially explored. We regard FactSage as promising but not yet applicable to most CAIs or Al-rich chondrules. *Hashimoto* (1991) also used a quasichemical model in a preliminary report on modeling activities in CMAS and achieved fairly good agreement with silica and CaO activities determined by *Rein and Chipman* (1965). MTDATA (*Davies et al., 2002*) is a program with associated databases developed at the National Physical Laboratory in the United Kingdom for calculating phase equilibria in a wide variety of systems. There have been some forays into using MTDATA for modeling CMAS liquids using various molecules as end members (*Davies et al., 1994; Blundy et al., 1996*), but the quality and range of applicability is difficult to gauge based on published results.

3.4. Trace-Element Partitioning

Trace-element systematics are useful recorders of igneous and metamorphic processes. In CAIs and Al-rich inclusions, trace-element distributions within a crystal may reflect simple closed-system fractional crystallization from an initially homogeneous droplet, but the system may also be characterized by significant exchange/volatilization. Complications that need to be considered in applying partition coefficients to CAI data include the possible influence of rapid crystal growth (*Kennedy et al., 1997*), sector zoning (*Hutcheon et al., 1978; Steele et al., 1997*), crystallization into a liquid of heterogeneous composition due to volatilization (e.g., *Richter et al., 2002*) or incomplete dissolution (*Kennedy et al., 1997*), subsolidus reequilibration with another primary or secondary phase and/or diffusive homogenization (*Meeker et al., 1983; Connolly et al., 2003*), and multiple heating and secondary alteration events (*MacPherson and Davis, 1993; Beckett et al., 2000*). This may seem a depressing litany of potential complications, but the complications also contain information concerning multiple processes. The study of trace-element distributions within CAIs continues to produce new insights into CAI evolution based on our understanding of the partitioning behavior of trace elements between crystals and CAI-like liquids in controlled conditions.

In this section, we consider crystal/liquid partitioning mostly for trace elements and we emphasize experimental

data obtained for essentially CMAS or CMAST liquids containing less than 1 wt% Na₂O. We also ignore data produced through optical beta autoradiography (Hoover, 1978) as there are substantial problems with the technique (Tingle, 1987; Beattie, 1993). General compilations/reviews of experimentally determined partition coefficients include Irving (1978), Green (1994), Jones (1995), and Wood and Blundy (2004).

Equilibrium partitioning of trace elements between crystals and liquid can be described in terms of exchange equilibria. If, for example, a trace amount of La substitutes into the M1 site of melilite (mel), then at equilibrium, a reaction $\text{LaO}_{3/2(\text{liq})} + \text{Ca}_2\text{Al}_2\text{SiO}_7(\text{mel}) + \text{MgO}_{(\text{liq})} = \text{CaO}_{(\text{liq})} + \frac{1}{2}\text{Al}_2\text{O}_3(\text{liq}) + \text{CaLaMgAlSiO}_7(\text{mel})$ can be written using oxide components for the liquid and gehlenite, a usually major component in melilite. This has a free energy of reaction

$$G_{\rightarrow} = 0 = G^{\circ}_{\rightarrow} + RT \ln \left[\frac{a_{\text{CaO}}^{\text{liq}} (a_{\text{Al}_2\text{O}_3}^{\text{liq}})^{1/2} a_{\text{CaLaMgAlSiO}_7}^{\text{mel}}}{a_{\text{MgO}}^{\text{liq}} a_{\text{LaO}_{3/2}}^{\text{liq}} a_{\text{Ca}_2\text{Al}_2\text{SiO}_7}^{\text{mel}}} \right]$$

which can be rearranged to isolate the partition coefficient

$$D_{\text{La}}^{\text{mel/liq}} = \frac{W_{\text{La}}^{\text{mel}}}{W_{\text{La}}^{\text{liq}}} = \left[-\exp\left(\frac{G_{\rightarrow}^{\circ}}{RT}\right) \right] \left[\left(\frac{a_{\text{MgO}}^{\text{liq}}}{a_{\text{CaO}}^{\text{liq}} (a_{\text{Al}_2\text{O}_3}^{\text{liq}})^{1/2}} \right) (\gamma_{\text{LaO}_{3/2}}^{\text{liq}}) \right] \left[\left(a_{\text{CaAl}_2\text{SiO}_7}^{\text{mel}} \right) \left(\frac{1}{\gamma_{\text{CaLaMgAlSiO}_7}^{\text{mel}}} \right) \right] \left(\frac{1}{\Phi_{\text{La}}} \right) \quad (2)$$

where W_i^j and X_i^j are the wt% and mole fraction of i in phase j , $\gamma_i^j = a_i^j/X_i^j$ is the activity coefficient of component i in phase j . Φ_{La} is a conversion factor to transform the mole ratio to a weight ratio. Equation (2) illustrates the variables that influence the value of a partition coefficient. The right-hand side of equation (2) contains three bracketed terms. The first one has variables whose values depend on the selected standard state and temperature but not composition. Standard state free energies of formation and oxide fusion data required for G_{\rightarrow}° are usually poorly constrained, so this term tends to be folded in with other multiplicative constants in equation (2) and indirectly determined through experimentation. The second bracketed term contains activities of major components in the liquid (CaO, MgO, Al₂O₃) and an activity coefficient associated with trace La in the liquid. All these variables depend on the temperature and major-element composition of the melt. In principle, $\gamma_{\text{LaO}_{3/2}}^{\text{liq}}$ also depends on the concentration of La in the liquid but if, as is commonly assumed, trace elements in the liquid obey Henry's law, then $\gamma_{\text{LaO}_{3/2}}^{\text{liq}}$ is constant for any specific temperature and major-element chemistry of the melt. The fact that trace elements often strongly prefer one of two immiscible liquids (Watson, 1976; Ryerson and Hess, 1978) implies a significant liquid composition effect if the range

in composition is sufficiently large. Recent work emphasizing the role of liquid composition on partitioning includes Kohn and Schofield (1994), Ertel et al. (1997), and O'Neill and Eggins (2002). The third bracketed term contains activities for gehlenite and a trace La component in melilite. Values for these depend on the major-element chemistry of the melilite and the specific local environment for La in the melilite. The conversion factor Φ_{La} is a weak function of the major-element composition of both melilite and the liquid.

Equation (2) summarizes the basic problem facing all applications of trace-element partitioning. There may in principle be significant contributions from the compositions of both phases and from temperature. While it can be argued (e.g., O'Neill and Eggins, 2002) that the effect of temperature on equilibrium trace-element partitioning is a secondary factor for most magmatic systems, crystallization can occur over ranges of hundreds of degrees in CAIs and Al-rich chondrules, making a complete dismissal of temperature effects rather dangerous. Also, the relative effects of solid and liquid compositions upon partition coefficients remain controversial. Fortunately, many of the variables in equation (2) cancel out for ratios of partition coefficients for elements of the same valence that substitute into the same site (e.g., for La in melilite, this would mean other trivalent cations substituting into M1), as noted by Drake and Weill (1975).

The crystal-oriented perspective for computing trace-element partition coefficients dates to observations of Brixner (1967) and Onuma et al. (1968) that the partition coefficients of similar trace elements substituting into a given site are roughly parabolic functions of ionic radius. Brice (1975) found that a simple isotropic lattice-strain accompanying the substitution of an element into a site that it does not quite fit could account for the differences in partition coefficients observed by Brixner. Nash and Crecraft (1985) introduced Brice's theory to the geochemical literature, and Blundy and coworkers in a series of papers (Blundy and Wood, 1991, 1994, 2003; Hill et al., 2000; Wood and Blundy, 2001, 2004) have extended and greatly popularized it.

Table 1 presents a compilation of ranges for experimentally determined values of trace- and minor-element partition coefficients for phases pertinent to CAIs and Al-rich chondrules in near-CMAS or CMAST liquids. Major-element partition coefficients are given, where supplied by the authors, but no attempt was made to calculate values from compositions of coexisting phases or to extract them from phase diagrams. The table is intended to give the reader a gross sense for what information is available, not what should be used in a particular application. In particular, it should be kept in mind that many of these elements occur in more than one valence state, leading to sensitivity of the partition coefficients to redox conditions. Specific values for selected elements for different crystalline phases are discussed below.

3.4.1. Oxides. To our knowledge, experimentally determined trace-element partition coefficients are not available for CaAl₂O₄ or grossite while for corundum, there is but one datum, a preliminary value of 0.12 for Sm in a CAS

TABLE 1. Ranges of experimentally determined partition coefficients.

Element	Anorthite	Clinopyroxene	Corundum	Hibonite	Melilite	Olivine	Perovskite	Protoenstatite	Spinel
Al	1.5–2.0	0.11–0.39		2.2		0.003–0.02	0.07–0.11		
Ba	0.06–0.26	0.003–0.02		0.03	0.025–0.050		0.03		
Be	0.90				0.5–1.8				
Ca	0.7–1.4	0.9–1.2		0.3		0.02–0.05	1.2	0.03	
Co	0.02	0.4–1.4							
Cr	0.016	2–34				0.3–0.8	0.63	1–4.5	
Cs									
Cu						0.27–0.47			
Fe	0.09	0.8–2.3							
Ga	0.8–1.0	0.19–0.24				0.012–0.018			
Ge	0.47–0.56	1.0–4.9		0.74–0.81		0.06–0.8	2.1		0.11
Hf		0.4–6.3		0.67–0.78			5		
In		1.3–2.8							
Li	0.23	0.03–0.21							
Mg	0.001–0.11	1.1		0.05		1.8–6.3	0.01–0.03	2.15	
Mn		0.68–0.80				0.5–0.7			
Mo		0.001–0.005							
Na	0.17–0.57	0.05–3			0.4–2.0				
Nb		0.006–0.07		0.18–0.35			2.7		
Ni		1.9–3.1				4–11		2.1	
Pd									<0.02
Rh		0.23–0.27							78–90
Ru		1.0–4.3							22–29
Sb		0.08–1.7							
Sc	0.012	0.35–29		0.31–0.50	0.01–0.07		0.16		0.05
Si	0.85			0.003–0.06			0.01		0.0006–0.002
Sn		2–29							
Sr	0.9–1.2	0.05–0.08		0.52–0.64	0.65–1.1		0.7–1.1		
Ta		0.02–0.41							
Th		0.01		0.7–1.2			16		
Ti	0.03–0.04	0.1–1.4		0.8–2.1	0.02		2.4		0.04–2.0
U	0.01	0.003–0.009		0.07–0.09			4.7		
V		0.01–0.15					1		~0–2.2
W		0.0003–0.005							
Y	0.003–0.03	0.6–0.9			0.015–0.09		1.1–1.9		
Zr	0.0003–0.0005	0.2–2.4		0.33–0.36	0.001–0.002		0.16–0.58		
La	0.02–0.17	0.07–0.16		4.9–7.2	0.04–0.48		2.6–15		0.01
Ce	0.07–0.10	0.08–0.27		3.9–5.2	0.06–0.21		11.6		
Pr	0.09	0.26–0.41		3.3–4.4			12		
Nd	0.08–0.10	0.18–0.51		2.8–3.5			13.4		
Sm	0.007–0.08	0.05–0.92	0.12	1.6–3.1	0.032–0.75		2.7–17		0.006
Eu	0.05–0.10	0.2–1.0		1.2–1.6	0.6–1.3		2.0–7.6		0.006
Gd	0.05	0.2–1.1		0.9–1.6	1.2		2.6–4.4		
Tb		1.04		0.52–0.76	0.49		1.6–3.6		0.008
Dy	0.02–0.03	0.23–1.07		0.35–0.41			3.6		
Ho		0.77–0.94		0.25–0.27			2.5		
Er	0.01–0.04	0.22–0.76		0.17–0.26			1.6		
Tm	0.03	0.7–1.1		0.10–0.13	0.03–0.14		1.2		
Yb	0.002	0.2–1.0		0.03–0.1	0.009–0.25		0.5–17		0.008
Lu	0.02–0.42	0.26–0.83		0.02–0.09	0.24		0.4–0.7		0.021

In addition to references cited in Irving (1978), Green (1994), Jones (1995), and Wood and Blundy (2004), data were drawn from Beckett and Stolper (1994, 2000), Connolly and Burnett (2003), Davis et al. (1996), Drake (1981), Hanson and Jones (1998), Kennedy et al. (1994), Libourel (1999), Miller et al. (2003), Pack and Palme (2003), Peters et al. (1995), Schreiber (1979), Simon et al. (1994a, 1996b), Soular et al. (1992), Steele et al. (1997), Terakado and Masuda (1979), Watson (1977), and Woolum et al. (1988).

liquid (Drake, 1981). Trace-element partitioning data for spinel are less sparse but not very systematic. In CMAS liquids, Malvin and Drake (1987) reported $D_{\text{Ge}}^{\text{sp/liq}} = 0.1$ while Capobianco and Drake (1990) found, in air, that Pd is highly incompatible ($D_{\text{Pd}}^{\text{sp/liq}} < 0.02$) and Rh and Ru highly compatible ($D_{\text{Rh}}^{\text{sp/liq}} > 20$). Malvin and Drake (1987) obtained $D_{\text{Ga}}^{\text{sp/liq}} = 4\text{--}5$ for spinels with ~1 wt% Fe_2O_3 . For the tran-

sition elements, data are quite limited. Connolly and Burnett (2003) obtained $D_{\text{Ti}}^{\text{sp/liq}} = 0.04$ for CAI-like liquids in air but 0.20 at the C-CO buffer (CCO), which they attributed to the stabilization of Ti^{3+} under reducing conditions. Their data for $D_{\text{V}}^{\text{sp/liq}}$ also show a strong f_{O_2} effect, ranging from ~0 in air to 2.2 at IW to 1.4 at CCO. Under oxidizing conditions, Cr^{3+} is so soluble in spinel that pichrochromites

(nominally MgCr_2O_4) coexist with otherwise CMAS liquids containing 0.1–0.2 wt% Cr as Cr_2O_3 (Hanson and Jones, 1998). The solubility of Cr in spinel under reducing conditions, where Cr^{2+} is likely dominant in the liquid (Schreiber *et al.*, 1978), does not appear to have been studied. Nagasawa *et al.* (1980) studied Sc and REE partitioning using INAA analysis of separates for an MAS liquid. All were reported to be incompatible but the $D_{\text{REE}}^{\text{sp/liq}}$ form an odd concave-up pattern as a function of ionic radius. Contamination of the spinel separate by glass cannot account for this effect. On the other hand, significant contamination by forsterite, which has partition coefficients for the heavy REE, $D_{\text{HREE}}^{\text{forst/liq}}$, much higher than those for the light REE, $D_{\text{LREE}}^{\text{forst/liq}}$ (e.g., Jones, 1995), could generate the observed pattern as ~40% of the solid phase assemblage in Nagasawa *et al.*'s (1980) experiment which would, according to the MAS phase diagram, have been olivine. If olivine contamination was in fact a problem with no significant contributions from glass, then $D_{\text{LREE}}^{\text{sp/liq}}$ given by Nagasawa *et al.* (1980) are a little low while those for Sc and the HREE are probably much higher than the correct values. An alternative is that the reported partition coefficients capture the true values for spinel. If so, perhaps the REE substitute into two different sites in spinel, with LREE preferring one and HREE preferring the other, or they substitute into the same site but with local charge balance and/or structural distortions being accommodated differently.

Hibonite has received more thorough study than spinel or corundum. Drake and Boynton (1988) determined the partitioning behavior of Sr and various REE between hibonite and CMAS liquids; samples were doped with several wt% of the “trace” elements and analyzed by EPMA. Kennedy *et al.* (1994) determined hibonite/liquid partition coefficients for an extensive suite of trace elements under reducing conditions. Doping levels were tens to hundreds of ppmw, with analysis by SIMS. $D_i^{\text{hib/liq}}$ for the two studies are broadly similar and, given the high doping concentrations and absence of Ti in the experiments of Drake and Boynton (1988), in good agreement. According to Kennedy *et al.* (1994), $D_{\text{Th}}^{\text{hib/liq}} \gg D_{\text{U}}^{\text{hib/liq}}$, which implies that slowly crystallized igneous hibonite should have strongly fractionated Th/U relative to the liquid. They also noted that, when plotted as a function of ionic radius, $D_{\text{Th}}^{\text{hib/liq}}$ and $D_{\text{U}}^{\text{hib/liq}}$ are near the REE and suggested that these elements substitute into the Ca site. Interestingly, $D_i^{\text{hib/liq}}$ for U, Th, and the trivalent REE at a given ionic radius are higher than those of divalent cations substituting into the Ca site, which is the opposite of expectations based solely on charge (Wood and Blundy, 2001) and observed in clinopyroxene (e.g., Hill *et al.*, 2000). Kennedy *et al.* (1994) attributed this to short-range order of compensating cations in nearby sites. They also found that $D_i^{\text{hib/liq}} > 1$ for the LREE, while middle and HREE are incompatible, with $D_{\text{La}}^{\text{hib/liq}}/D_{\text{Lu}}^{\text{hib/liq}} \sim 200$. Thus, igneous hibonite should be LREE-enriched relative to the liquid from which it crystallized and HREE-depleted unless crystallization was so rapid that all the $D_i^{\text{hib/liq}}$ approached 1. Small, highly charged cations (Si, Ge, Hf, Zr, Ti) and the

trivalent transition elements (e.g., Sc) except for Ti are moderately to highly incompatible (Drake and Boynton, 1988; Beckett and Stolper, 1994; Kennedy *et al.*, 1994).

The overall pattern of trace-element partitioning between perovskite and liquid (Kennedy *et al.*, 1994; Corgne and Wood, 2002) as a function of ionic radius is qualitatively similar to that of hibonite, in that trivalent and quadrivalent cations substituting into the Ca site are more compatible than divalent cations of the same ionic radius and the phase prefers light over heavy REE. Based on data of Kennedy *et al.* (1994), however, $D_{\text{LREE}}^{\text{pv/liq}}/D_{\text{HREE}}^{\text{pv/liq}} \sim 10$ (vs. 200 for hibonite), $D_{\text{Th}}^{\text{pv/liq}}/D_{\text{U}}^{\text{pv/liq}} \sim 3$ (vs. 8–17 for hibonite), and generally $D_i^{\text{pv/liq}}/D_i^{\text{hib/liq}} > 1$ for high field strength elements. Literature determinations of $D_{\text{REE}}^{\text{pv/liq}}$ (Ringwood, 1975; Nagasawa *et al.*, 1980; Kennedy *et al.*, 1994; Simon *et al.*, 1994a) agree only within factors of 6 (La, Sm) to 35 (Yb). Simon *et al.* (1994a) suggest that these differences reflect differing Al contents of the liquid and oxygen fugacities. The former, or some crystal composition parameter strongly correlated with Al in the liquid, appears to be the dominant factor. Figure 8a shows values of $\text{RTln}D_{\text{La}}^{\text{pv/liq}}$ (R in terms of kJ) as a function of $X_{\text{Al}_2\text{O}_3}^{\text{liq}}$, the mole fraction of Al_2O_3 in the liquid, with all Ti as Ti^{4+} . All the CMAST data, regardless of whether experiments were conducted under oxidizing or reducing conditions, are consistent with a single linear trend in spite of major differences in liquid composition. This implies that $D_{\text{La}}^{\text{pv/liq}}$ can be treated as a simple function of Al_2O_3 concentration in the liquid; since Nagasawa *et al.*'s (1980) value for a CST liquid lies well below the regression, the simple functionality must break down at low Al_2O_3 . Analogous plots for Sm and Yb show similar systematics. For CAIs, which are invariably aluminous, suitable values for $D_{\text{REE}}^{\text{pv/liq}}$ of Y and other trivalent REE can be inferred from $D_{\text{La}}^{\text{pv/liq}}$ through an unweighted fit of Kennedy *et al.*'s (1994) data to Blundy and Wood's (1994) expression converted to log form

$$\text{RTln}(D_i^{\text{pv/liq}}/D_{\text{La}}^{\text{pv/liq}}) = -1614 \left\{ (r_{\text{La}}^{\text{pv/liq}})^2 - (r_i^{\text{pv/liq}})^2 \right\} - 944.6 \left\{ (r_i^{\text{pv/liq}})^3 - (r_{\text{La}}^{\text{pv/liq}})^3 \right\} \quad (3)$$

where following Corgne and Wood (2002) we use ionic radii for 8-coordinated sites. The Ca site in perovskite is actually 12-coordinated, but appropriate radii are not available for all the REE. The possible influence of liquid composition on partitioning for other trace elements is unknown. The experimental database for $D_i^{\text{pv/liq}}$ is nevertheless good enough to provide a strong test of igneous partitioning for perovskites in CAIs (e.g., Davis and Grossman, 1979; Simon *et al.*, 1994a, 1996a, 1999).

3.4.2. Silicates. Experimentally determined partitioning data are available for three phases, anorthite, olivine, and melilite, that crystallized from melts in at least some CAIs. No experimental data are available for fassaite but there is a substantial database for aluminous clinopyroxenes in equilibrium with CMAS liquids, and Simon *et al.* (1991)

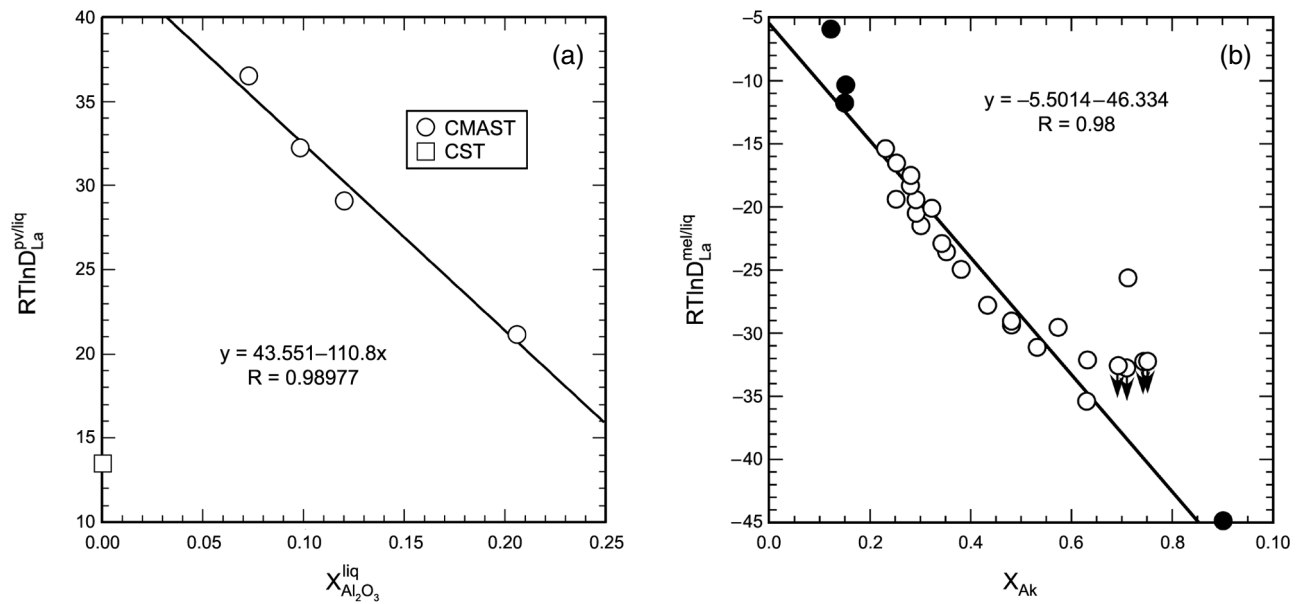


Fig. 8. Partitioning of La between crystals and liquid. (a) $RT \ln D_{La}^{p/liq}$ (R in terms of kJ) as a function of $X_{Al_2O_3}^{liq}$. CMAST data are from Ringwood (1975), Kennedy et al. (1994), and Simon et al. (1994a) and CST data from Nagasawa et al. (1980). The line is an unweighted linear regression through the CMAST data. (b) $RT \ln D_{La}^{m/liq}$ (R in terms of kJ) as a function of X_{Ak} . Data are from Ringwood (1975), Nagasawa et al. (1980), Kuehner et al. (1989), Beckett et al. (1990), and Davis et al. (1996). Closed and open circles refer to compositions on and off the åkermanite-gehlenite join, respectively. The line is an unweighted linear regression to all data excluding that of Ringwood (1975), which lies well off the trend, and the upper limits, shown with arrows, from Beckett et al. (1990).

used observed abundances in fassaite from type B inclusions to infer partition coefficients.

Plagioclase has been the subject of several partitioning studies in CMAS liquids. Using a CAI-like liquid as a base composition, Simon et al. (1994a) doped samples with several wt% total of Sr, Zr, La, Sm, and Yb oxides and determined $D_1^{an/liq}$ using EPMA and SIMS. Except for Sr ($D_{Sr}^{an/liq} = 1.0$), all these elements, along with Mg and Ti^{4+} ($D_{Ti^{4+}}^{an/liq} = 0.03$), are highly incompatible in plagioclase. Peters et al. (1995) obtained similar results for Mg and Ti^{4+} , inferred $D_{Ti^{3+}}^{an/liq} \sim 0.04$, and concluded that both Ti^{3+} and Ti^{4+} are probably in tetrahedral coordination. Barium (Miller et al., 2003), Ga, Ge (Malvin and Drake, 1987), and Na (Soullard et al., 1992; Beckett and Stolper, 2000) are moderately incompatible. Early work suggesting a Henry's law effect for trace-element partitioning at very low concentrations such that $D_{REE}^{an/liq}$ increased dramatically at low concentrations (e.g., Hoover, 1978) are apparently due to analytical artifacts (Beattie, 1993), but Bindeman and Davis (2000) observed similar effects in some experiments involving sodic plagioclase (An_{45-75}) based on SIMS analyses, with increases of up to a factor of 2 between low (~ 1 ppm) and high (100 to several hundred ppm) concentrations in plagioclase. They observed no Henry's law effect for Sr-doped experiments and no effect for elements other than the REE.

Experimentally determined $D_{Mg}^{an/liq}$ are rather variable. Some of Malvin and Drake's (1987) data imply $D_{Mg}^{an/liq} \sim 0.001$, although this is probably an analytical artifact given the low concentrations in plagioclase; most experimentally

determined $D_{Mg}^{an/liq}$ are in the range 0.01–0.11 (Malvin and Drake, 1987; Peters et al., 1995; Steele et al., 1997; Beckett and Stolper, 2000; Miller et al., 2003). Much of this range probably reflects differences in liquid composition (Peters et al., 1995; Simon et al., 1994a; Steele et al., 1997) and some may reflect activation volumes for plagioclase analyses extending through the often thin, tabular, feldspar crystals. A complicating factor for the interpretation of both experimental and meteoritic data is that the anorthite is frequently sector-zoned (Hutcheon et al., 1978; Steele et al., 1997), with concentrations of Mg and Na differing by up to a factor of 2 across sector boundaries. Possible sector-zoning effects for elements other than Mg, Na, and Ti do not appear to have been examined. Finally, it should be mentioned that fits for plagioclase-liquid partitioning of trace elements in more sodic and magmatic systems than considered here (Blundy and Wood, 1991; Bindeman et al., 1998; Bindeman and Davis, 2000) can be extrapolated to anorthite. Agreement with the above-mentioned CMAS and CMAST studies ranges from fairly good (Na, Mg, Ti) to very bad (REE). Since these expressions include many elements (e.g., Be, Co, Fe, Li, U) for which there are currently no experimental data involving CAI-like liquids, they are nevertheless still worth using if a general idea of compatibility is desired.

Olivine is a major phase in terrestrial rocks and its partitioning behavior in magmatic systems has received considerable attention (e.g., Irving, 1978; Green, 1994; Jones, 1995; Wood and Blundy, 2004). With, however, the notable

exception of Ca (*Libourel, 1999*), Ga and Ge (*Capobianco and Watson, 1982; Malvin and Drake, 1987*), and some of the transition elements (*Watson, 1977; Hart and Davis, 1978; Schreiber, 1979; Hanson and Jones, 1998; Dudnikova et al., 2001*), most data refer to Fe-bearing systems, although extrapolation to forsterite is often possible (e.g., *Jones, 1995*). Perhaps the most immediately relevant data for CAIs is the correlation between $D_{Ca}^{ol/liq}$ and CaO content of the liquid (*Libourel, 1999*). The relationship holds well for CMAS, CMAST, and CMAS + Cr liquids (*Libourel, 1999*), and *Pack and Palme (2003)* found no discernible effect for high cooling rates. The addition of Na to the liquid leads to higher values of $D_{Ca}^{ol/liq}$ than expected based on *Libourel's (1999)* equation, but this is negligible for <2 wt% Na₂O, the range of interest for CAIs. Although it has not been used for this purpose, the Ca content of olivine from type B3 (olivine-bearing) CAIs may be a powerful monitor of liquid composition.

Experimentally determined $D_i^{mel/liq}$ for melilite are available for minor or trace amounts of Ba, Be, Na, Sc, Sr, Ti, Y, Zr, and the REE (*Ringwood, 1975; Nagasawa et al., 1980; Kuehner et al., 1989; Beckett et al., 1990; Souillard et al., 1992; Davis et al., 1996; Simon et al., 1996b; Beckett and Stolper, 2000*). Unlike olivine and anorthite in CAIs, whose variations in major-element chemistry are small and whose compositions therefore have little impact on partitioning, melilite is essentially a binary solid solution in CAIs and, where charge-compensating substitutions are required, there is a strong dependence of $D_i^{mel/liq}$ on the major-element composition, or X_{Ak} . An example is shown for La, which substitutes into the Ca site, in Fig. 8b. Data for Y and the other REE show similar relationships between $D_i^{mel/liq}$ and X_{Ak} . $D_{La}^{mel/liq}$ varies by nearly a factor of 20 but, with the exception of one datum from *Ringwood (1975)*, all the data are consistent with the line shown in Fig. 8b. It is possible the aberrant $D_{La}^{mel/liq}$ reflects a liquid composition effect as the bulk composition, which was based on a mixture of melilite and a CAI pyroxene composition from *Mason and Martin (1974)*, is significantly different from those of other studies (pyroxene-rich vs. compositions along the join åkermanite-gehlenite, and spinel-poor relative to CAI-like compositions) or even a typo (if $D_{La}^{mel/liq}$ were 0.05 instead of 0.15, the point would have plotted near the line). In any case, suitable $D_{La}^{mel/liq}$ for CAIs can be obtained from Fig. 8b without resolving the relevance of *Ringwood's* data. Values for other trivalent REE can be obtained from an unweighted regression of Y and trivalent REE data from *Davis et al. (1996)* for $X_{Ak} = 0.23$ melilite, giving

$$RT \ln(D_i^{mel/liq}/D_{La}^{mel/liq}) = -1155 \left\{ (r_{La}^{mel/liq})^2 - (r_i^{mel/liq})^2 \right\} - 692.8 \left\{ (r_i^{mel/liq})^3 - (r_{La}^{mel/liq})^3 \right\} \quad (4)$$

(see discussion of *Wood and Blundy, 2004*). All the trivalent REE are predicted to be incompatible in melilite with

$D_{REE}^{mel/liq}$ generally decreasing with increasing X_{Ak} . Beryllium has the opposite behavior with $D_{Be}^{mel/liq}$ increasing with increasing X_{Ak} such that Be changes from incompatible to compatible with increasing degree of crystallization in a CAI-like bulk composition (*Beckett et al., 1990*). Based on Sc data of *Nagasawa et al. (1980)* and *Beckett et al. (1990)*, $RT \ln D_{Sc}^{mel/liq} = -32.04 - 65.4 X_{Ak}$ for $X_{Ak} < 0.36$ and $-58 + 6.71 X_{Ak}$ for $X_{Ak} > 0.36$ (R being the gas constant in kJ). Scandium probably has a different dominant substitution mechanism in aluminous vs. magnesian melilites. Barium and Sr substitute into the Ca site. $D_{Ba}^{mel/liq}$ is 0.02–0.04 (*Beckett et al., 1990; Simon et al., 1994a*) and $D_{Sr}^{mel/liq}$ is probably ~0.7 (*Nagasawa et al., 1980; Woolum et al., 1988; Kuehner et al., 1989; Simon et al., 1996b*), although values as high as 1.1 have been reported (*Ringwood, 1975; Kuehner et al., 1989*). $D_i^{mel/liq}$ for Ba and Sr are essentially independent of X_{Ak} (*Beckett et al., 1990; Simon et al., 1994a*). *Simon et al. (1996b)* obtained $D_{Ti^{4+}}^{mel/liq} = 0.020$. Finally, Na deserves special mention. As a trace constituent, Na behaves similarly to Be (*Beckett and Stolper, 2000*), increasing with increasing X_{Ak} by a factor of nearly 4 between $X_{Ak} = 0.22$ ($D_{Na}^{mel/liq} = 0.4$) and $X_{Ak} = 0.65$ ($D_{Na}^{mel/liq} = 1.5$) for CAI-like liquids. As Na₂O in the liquid is increased to more than a few tenths of a wt%, the influence of liquid composition becomes more apparent, and *Beckett and Stolper (2000)* appealed to both crystal-chemical and liquid composition effects in modeling available Na partitioning data (*Pan and Longhi, 1989, 1990; Souillard et al., 1992; Krigman et al., 1995; Beckett and Stolper, 2000*).

While a fairly extensive collection of data exists on trace-element partitioning for clinopyroxenes with compositions close to the join diopside-CaTschermarks, references for which can be found in the reviews of *Irving (1978)*, *Green (1994)*, and *Wood and Blundy (2004)*, there are no experimentally determined $D_i^{fass/liq}$ for the compositionally complex fassaite observed in CAIs. Probably the best option at present is to use apparent $D_i^{fass/liq}$ derived by *Simon et al. (1991)* from three type B1 CAIs. Their model values for Y, REE, Sc, Zr, Hf, and Ta are within the range observed experimentally for Di-CaTs pyroxenes; their model $D_i^{fass/liq}$ for U and Th are lower than obtained by *Benjamin et al. (1980)* and *LaTourette and Burnett (1992)*, and the model $D_{Nb}^{fass/liq}$ is higher than values obtained by *Lundstrom et al. (1998)* and *Hill et al. (2000)*. In addition to significant differences in the pyroxene compositions, there may also be different valence states in CAI liquids and pyroxenes relative to the experiments. According to the model of *Simon et al. (1991)*, Sc, Zr, and Hf are compatible; Nb, Ta, Y, and the REE are moderately incompatible; and U and Th are highly incompatible.

3.5. Dynamic Crystallization Experiments

In previous sections, the primary focus was on tools that can be used for the exploration of phase equilibria of CAI-like liquids and equilibrium constraints on the crystallization of these objects if they were partially or completely

melted. This is important, but crystallization of a CAI is an inherently dynamic process. The effect of kinetic processes on the observed phase assemblages and their compositions is constrained through equilibrium phase diagrams and thermodynamic calculations in the sense that boundary conditions at crystal-liquid surfaces and perfect fractional crystallization paths can be determined, metastable extensions of stability fields can be used to help establish liquid lines of descent if a stable phase fails to nucleate, liquid compositions can be constrained from the crystalline phase compositions, and the conditions under which a crystal dissolves and whether or not that dissolution is likely to be congruent (the phase dissolves directly into the melt) or incongruent (one or more crystalline phases form between the original dissolving phase and the liquid) can be predicted (Cooper, 1970; Zhang and Lee, 2000).

A formal consideration of transport properties in the liquid and/or vapor is required to flesh out time and chemical evolution (see, e.g., Grossman et al., 2000; Richter et al., 2002; Davis and Richter, 2004). Some useful constraints on process can also be obtained through dynamic crystallization and partial melting experiments without understanding much about the processes producing the phases, but great care is required to avoid categorical statements based on them because the results are almost always permissive, especially where textural observations are involved (i.e., different sets of conditions not explored in the experiments could lead to a similar result).

The experimental database for chondrules is heavily weighted by dynamic crystallization experiments of one sort or another and the results have strongly influenced thinking about these objects (e.g., Connolly and Hewins, 1996; Hewins and Connolly, 1996; Connolly and Desch, 2004). In the CAI literature, there is only one really influential classical dynamic crystallization study, that of Stolper and Paque (1986). They conducted a series of single-stage, dynamic crystallization experiments on one bulk composition typical of type B CAIs, in which the sample was held at a maximum temperature for a specified period of time, cooled at a constant rate, and then quenched at a specific temperature. They found that fast cooling rates ($>100^{\circ}\text{C}/\text{h}$) and maximum temperatures (T_{max}) significantly above the appearance of melilite (1390°C for their bulk composition) led to dendritic melilite and significant Mg-Tschermaks component in pyroxene, neither of which is observed in type Bs (but see Simon et al., 1998), leading to the conclusion that type B CAIs probably cooled more slowly. MacPherson et al. (1984b) had already shown for the same bulk composition that cooling rates faster than $50^{\circ}\text{C}/\text{h}$ would lead exclusively to normally zoned melilites in which compositions become progressively more magnesian from core-to-rim. Reversals back toward more aluminous melilites were observed by MacPherson et al. (1984b) in melilites grown at cooling rates less than $50^{\circ}\text{C}/\text{h}$ and since reversely zoned melilites are commonly observed in type B1 CAIs, MacPherson et al. concluded that cooling rates for these CAIs were slower than $\sim 50^{\circ}\text{C}/\text{h}$. Later single- and multiple-

stage dynamic crystallization experiments designed to reproduce textures (Maharaj and Hewins, 1994; Paque, 1995) and trace-element partitioning (Davis et al., 1996; Simon et al., 1996b) of CAIs have not changed the basic constraints established in these two papers, although the influence of “flash heating” (Maharaj and Hewins, 1995), precursor materials (Paque, 1995; Maharaj and Hewins, 1997), remelting (Paque et al., 1998, 2000), and nonlinear cooling paths have not been fully explored. Production of the mineral “UNK” in dynamic crystallization experiments on various CAI-like compositions if cooling rates were less than a few tens of degrees per hour but not at faster rates (Paque et al., 1994) is also consistent with a maximum cooling rate in the range of several tens of degrees per hour. In an interesting set of experiments, Mendybaev et al. (2003) found that a continuous melilite mantle, the basic defining characteristic of type B1 inclusions, could be produced by cooling a CAI-like composition in a flowing H_2 gas at $5^{\circ}\text{C}/\text{h}$ but that no mantle was produced in a similar sample cooled at $10^{\circ}\text{C}/\text{h}$. They suggested that the difference between type B1 and B2 inclusions was essentially the difference between relatively faster (B2) and more slowly (B1) cooled droplets. Overall, data from all these studies are consistent with cooling rates of a few to a few tens of degrees per hour for type B CAIs at $\sim 1300^{\circ}\text{--}1400^{\circ}\text{C}$. Stolper and Paque (1986) suggested a lower limit of a few tenths of a degree per hour near the appearance temperature of plagioclase based on the premise that slower rates would *always* lead to the appearance of plagioclase before fassaite, whereas the opposite is frequently inferred for type Bs (MacPherson et al., 1984b). There is growing evidence that many type B CAIs were partially melted more than once (MacPherson and Davis, 1993; Beckett et al., 2000; Connolly and Burnett, 2003) and some experimental evidence (Paque et al., 2000) that multiple melting events enhance the probability of producing coarse-grained plagioclase before pyroxene, but this order of crystallization constraint should probably be viewed as qualitative at present.

Acknowledgments. We are grateful to J. Paque and S. B. Simon for their reviews of the manuscript, as well as the comments of S. Krot and D. S. Lauretta. This work was supported in part by grants from PSC CUNY (H.C.C., PI) and NASA.

REFERENCES

- Agamawi Y. M. and White J. (1953) The quaternary system $\text{CaO-Al}_2\text{O}_3\text{-TiO}_2\text{-SiO}_2$ Part I. — The ternary system anorthite-sphene-silica. *Trans. British Cer. Soc.*, 52, 271–310.
- Agamawi Y. M. and White J. (1954a) The quaternary system $\text{CaO-Al}_2\text{O}_3\text{-TiO}_2\text{-SiO}_2$ Part II. — The ternary system calcium metasilicate-sphene-silica. *Trans. British Cer. Soc.*, 53, 1–22.
- Agamawi Y. M. and White J. (1954b) The quaternary system $\text{CaO-Al}_2\text{O}_3\text{-TiO}_2\text{-SiO}_2$ Part III. — The quaternary system calcium metasilicate-anorthite-sphene-silica. *Trans. British Cer. Soc.*, 53, 23–38.
- Anderson G. M. and Crerar D. A. (1993) *Thermodynamics in Geochemistry: The Equilibrium Model*. Oxford Univ., Oxford, 588 pp.

- Bale C. W., Chartrand P., Degterov S. A., Eriksson G., Hack K., Ben Mahfoud R., Melancon J., Pelton A. D., and Petersen S. (2002) FactSage thermochemical software and databases. *Calphad*, 26, 189–228.
- Ban-ya S. (1993) Mathematical expression of slag-metal reactions in steelmaking process by quadratic formalism based on the regular solution model. *ISIJ Intl.*, 33, 2–11.
- Barron L. M. (1985) Comment on “A thermodynamic model for multicomponent melts, with application to the system CaO-Al₂O₃-SiO₂” by Berman and Brown. *Geochim. Cosmochim. Acta*, 49, 611–612.
- Bartels K. S. and Grove T. L. (1991) High-pressure experiments on magnesian eucrite compositions: Constraints on magmatic processes in the eucrite parent body. *Proc. Lunar Planet. Sci. Conf.*, Vol. 21, pp. 351–365.
- Beattie P. (1993) On the occurrence of apparent non-Henry’s Law behaviour in experimental partitioning studies. *Geochim. Cosmochim. Acta*, 57, 47–55.
- Beckett J. R. and Grossman L. (1988) The origin of type C inclusions from carbonaceous chondrites. *Earth Planet. Sci. Lett.*, 89, 1–14.
- Beckett J. R. and Stolper E. (1994) The stability of hibonite, melilite and other aluminous phases in silicate melts: Implications for the origin of hibonite-bearing inclusions from carbonaceous chondrites. *Meteoritics*, 29, 41–65.
- Beckett J. R. and Stolper E. (2000) The partitioning of Na between melilite and liquid: Part I. The role of crystal chemistry and liquid composition. *Geochim. Cosmochim. Acta*, 64, 2509–2517.
- Beckett J. R., Spivack A. J., Hutcheon I. D., Wasserburg G. J., and Stolper E. M. (1990) Crystal chemical effects on the partitioning of trace elements between mineral and melt: An experimental study of melilite with applications to refractory inclusions from carbonaceous chondrites. *Geochim. Cosmochim. Acta*, 54, 1755–1774.
- Beckett J. R., Paque J. M., and Stolper E. M. (1999) The use of melilite compositions to constrain the thermal history and liquid line of descent of Type B CAIs (abstract). In *Lunar and Planetary Science XXX*, Abstract # 1920. Lunar and Planetary Institute, Houston (CD-ROM).
- Beckett J. R., Simon S. B., and Stolper E. (2000) The partitioning of Na between melilite and liquid: Part II. Applications to Type B inclusions from carbonaceous chondrites. *Geochim. Cosmochim. Acta*, 64, 2519–2534.
- Benjamin T., Heuser W. R., Burnett D. S., and Seitz M. G. (1980) Actinide crystal-liquid partitioning for clinopyroxene and Ca₃(PO₄)₂. *Geochim. Cosmochim. Acta*, 44, 1251–1264.
- Berman R. G. (1983) A thermodynamic model for multicomponent melts, with application to the system CaO-MgO-Al₂O₃-SiO₂. Ph.D. dissertation, Univ. of British Columbia.
- Berman R. G. and Brown T. H. (1984) A thermodynamic model for multicomponent melts, with application to the system CaO-Al₂O₃-SiO₂. *Geochim. Cosmochim. Acta*, 48, 661–678.
- Biggar G. M. (1971) Phase relationships of bredigite (Ca₅MgSi₃O₁₂) and of the quaternary compound (Ca₆MgAl₈SiO₂₁) in the system CaO-MgO-Al₂O₃-SiO₂. *Cement Concrete Res.*, 1, 493–513.
- Biggar G. M. (1984) The composition of diopside solid solutions, and of liquids, in equilibrium with forsterite, plagioclase, and liquid in the system Na₂O-CaO-MgO-Al₂O₃-SiO₂ and in remelted rocks from 1 bar to 12 kbar. *Mineral. Mag.*, 48, 481–494.
- Bindeman I. N. and Davis A. M. (2000) Trace element partitioning between plagioclase and melt: Investigation of dopant influence on partition behavior. *Geochim. Cosmochim. Acta*, 64, 2863–2878.
- Bindeman I. N., Davis A. M., and Drake M. J. (1998) Ion microprobe study of plagioclase-basalt partition experiments at natural concentration levels of trace elements. *Geochim. Cosmochim. Acta*, 62, 1175–1193.
- Bischoff A. and Keil K. (1983) Ca-Al-rich chondrules and inclusions in ordinary chondrites. *Nature*, 303, 588–592.
- Bischoff A. and Keil K. (1984) Al-rich objects in ordinary chondrites: Related origin of carbonaceous and ordinary chondrites and their constituents. *Geochim. Cosmochim. Acta*, 48, 693–709.
- Bischoff A., Keil K., and Stöffler D. (1985) Perovskite-hibonite-spinel-bearing inclusions and Al-rich chondrules and fragments in enstatite chondrites. *Chem. Erde*, 44, 97–106.
- Bischoff A., Palme H., Schultz L., Weber D., Weber H. W., and Spettel B. (1993) Acfer 182 and paired samples, an iron-rich carbonaceous chondrite: Similarities with ALH85085 and relationship to CR chondrites. *Geochim. Cosmochim. Acta*, 57, 2631–2648.
- Björkqvall J., Du S., and Seetharaman S. (2001) Thermodynamic model calculations in multicomponent liquid silicate systems. *Ironmaking Steelmaking*, 28, 250–257.
- Blum J. D., Wasserburg G. J., Hutcheon I. D., Beckett J. R., and Stolper E. M. (1989) Origin of opaque assemblages in C3V meteorites: Implications for nebular and planetary processes. *Geochim. Cosmochim. Acta*, 53, 543–556.
- Blundy J. D. and Wood B. J. (1991) Crystal-chemical controls on the partitioning of Sr and Ba between plagioclase feldspar, silicate melts, and hydrothermal solutions. *Geochim. Cosmochim. Acta*, 55, 193–209.
- Blundy J. D. and Wood B. J. (1994) Prediction of crystal-melt partition coefficients from elastic moduli. *Nature*, 372, 452–454.
- Blundy J. D. and Wood B. J. (2003) Partitioning of trace elements between crystals and melts. *Earth Planet. Sci. Lett.*, 210, 383–397.
- Blundy J. D., Wood B. J., and Davies A. (1996) Thermodynamics of rare earth element partitioning between clinopyroxene and melt in the system CaO-MgO-Al₂O₃-SiO₂. *Geochim. Cosmochim. Acta*, 60, 359–364.
- Bowen N. L. (1915) The crystallization of haplobasaltic, haplodioritic and related magmas. *Am. J. Sci.*, 190, 161–185.
- Bowen N. L. (1928) *The Evolution of the Igneous Rocks*. Princeton Univ., Princeton. 332 pp.
- Brearley A. J. and Jones R. H. (1998) Chondritic meteorites. In *Planetary Materials* (J. J. Papike, ed.), pp. 3-1 to 3-398. Reviews in Mineralogy, Vol. 36, Mineralogical Society of America.
- Brice J. C. (1975) Some thermodynamic aspects of the growth of strained crystals. *J. Crystal Growth*, 28, 249–253.
- Brixner L. H. (1967) Segregation coefficients of the rare earth niobates in CaMoO₄. *J. Electrochem. Soc.*, 114, 108–110.
- Capobianco C. J. and Drake M. J. (1990) Partitioning of ruthenium, rhodium, and palladium between spinel and silicate melt and implications for platinum group element fractionation trends. *Geochim. Cosmochim. Acta*, 54, 869–874.
- Capobianco C. J. and Watson E. B. (1982) Olivine/silicate melt partitioning of germanium: An example of a nearly constant partition coefficient. *Geochim. Cosmochim. Acta*, 46, 235–240.

- Chamberlin L., Beckett J. R., and Stolper E. (1994) Pd-oxide equilibration: A new experimental method for the direct determination of oxide activities in melts and minerals. *Contrib. Mineral. Petrol.*, 116, 169–181.
- Connolly H. C. and Burnett D. S. (2003) On type B CAI formation: Experimental constraints on f_{O_2} variations in spinel minor element partitioning and reequilibration effects. *Geochim. Cosmochim. Acta*, 67, 4429–4434.
- Connolly H. C. and Desch S. J. (2004) On the origin of the “kleine Kugelchen” called chondrules. *Chem. Erde*, 64, 95–125.
- Connolly H. C. and Hewins R. H. (1996) Constraints on chondrule precursors from experimental data. In *Chondrules and the Protoplanetary Disk* (R. H. Hewins et al., eds.), pp. 129–135. Cambridge Univ., Cambridge.
- Connolly H. C., Burnett D. S., and McKeegan K. D. (2003) The petrogenesis of type B1 Ca-Al-rich inclusions: The spinel perspective. *Meteoritics & Planet. Sci.*, 38, 197–224.
- Cooper A. R. (1970) The use of phase diagrams in dissolution studies. In *Phase Diagrams Materials Science and Technology, Vol. III* (A. M. Alper, ed.), pp. 237–251. Academic, New York.
- Corgne A. and Wood B. J. (2002) CaSiO₃ and CaTiO₃ perovskite-melt partitioning of trace elements: Implications for gross mantle differentiation. *Geophys. Res. Lett.*, 29(19), 1933, doi: 10.1029/2001GL014398, 2002.
- Davies A., Wood B., Barry T., Dinsdale A., and Gisby J. (1994) The thermodynamics of mineral-melt equilibria in the system CaO-MgO-Al₂O₃-SiO₂ (abstract). *Mineral. Mag.*, 58A, 213–214.
- Davies R. H., Dinsdale A. T., Gisby J. A., Robinson J. A. J., and Martin S. M. (2002) MTDATA — Thermodynamic and phase equilibrium software from the National Physical Laboratory. *Calphad*, 26, 229–271.
- Davis A. M. (2006) Volatile evolution and loss. In *Meteorites and the Early Solar System II* (D. S. Lauretta and H. Y. McSween Jr., eds.), this volume. Univ. of Arizona, Tucson.
- Davis A. M. and Grossman L. (1979) Condensation and fractionation of rare earths in the solar nebula. *Geochim. Cosmochim. Acta*, 43, 1611–1632.
- Davis A. M. and Richter F. M. (2004) Condensation and evaporation of solar system materials. In *Treatise on Geochemistry, Vol. 1: Meteorites, Comets, and Planets* (A. M. Davis, ed.), pp. 407–430. Elsevier, Oxford.
- Davis A. M., MacPherson G. J., Clayton R. N., Mayeda T. K., Sylvester P. J., Grossman L., Hinton R. W., and Laughlin J. R. (1991) Melt solidification and late-stage evaporation in the evolution of a FUN inclusion from the Vigarano C3V chondrite. *Geochim. Cosmochim. Acta*, 55, 621–637.
- Davis A. M., Richter F. M., Simon S. B., and Grossman L. (1996) The effect of cooling rate on melilite/liquid partition coefficients for Y and REE in Type B CAI melts (abstract). In *Lunar and Planetary Science XXVII*, pp. 291–292. Lunar and Planetary Institute, Houston.
- de Aza A. H., Pena P., and de Aza S. (1999) Ternary system Al₂O₃-MgO-CaO: I, Primary phase field of crystallization of spinel in the subsystem MgAl₂O₄-CaAl₄O₇-CaO-MgO. *J. Am. Ceramic Soc.*, 82, 2193–2203.
- de Aza A. H., Iglesias J. E., Pena P., and de Aza S. (2000) Ternary system Al₂O₃-MgO-CaO: II, Phase relationships in the subsystem Al₂O₃-MgAl₂O₄-CaAl₄O₇. *J. Am. Ceramic Soc.*, 83, 919–927.
- DeVries R. C. and Osborn E. F. (1957) Phase equilibria in high-alumina part of the system CaO-MgO-Al₂O₃-SiO₂. *J. Am. Ceramic Soc.*, 40, 6–15.
- DeVries R. C., Roy R., and Osborn E. F. (1955) Phase equilibria in the system CaO-TiO₂-SiO₂. *J. Am. Ceramic Soc.*, 38, 158–171.
- Drake M. J. (1981) Partitioning of Sm between hibonite and corundum and silicate melt (abstract). In *Lunar and Planetary Science XII*, pp. 235–236. Lunar and Planetary Institute, Houston.
- Drake M. J. and Boynton W. V. (1988) Partitioning of rare earth elements between hibonite and melt and implications for nebular condensation of the rare earth elements. *Meteoritics*, 23, 75–80.
- Drake M. J. and Weill D. F. (1975) Partition of Sr, Ba, Ca, Y, Eu²⁺, Eu³⁺, and other REE between plagioclase feldspar and magmatic liquid: An experimental study. *Geochim. Cosmochim. Acta*, 39, 689–712.
- Dudnikova V. B., Zharikov E. V., Eremin N. N., Zharkova E. V., Lebedev V. F., and Urusov V. S. (2001) Vanadium distribution between forsterite and its melt: The structural and oxidation state of vanadium. *Geochem. Intl.*, 39(7), 667–675.
- Ebel D. S. (2006) Condensation of rocky material in astrophysical environments. In *Meteorites and the Early Solar System II* (D. S. Lauretta and H. Y. McSween Jr., eds.), this volume. Univ. of Arizona, Tucson.
- Ebel D. S. and Grossman L. (2000) Condensation in dust-enriched systems. *Geochim. Cosmochim. Acta*, 64, 339–366.
- El Goresy A., Nagel K., and Ramdohr P. (1978) Fremdlinge and their noble relatives. *Proc. Lunar Planet. Sci. Conf. 9th*, pp. 1279–1303.
- El Goresy A., Palme H., Yabuki H., Nagel K., Herrwerth I., and Ramdohr P. (1984) A calcium-aluminum-rich inclusion from the Essebi (CM2) chondrite: Evidence for captured spinel-hibonite spherules and for an ultra-refractory rimming sequence. *Geochim. Cosmochim. Acta*, 48, 2283–2298.
- Ertel W., Dingwell D. B., and O’Neill H. S. C. (1997) Compositional dependence of the activity of nickel in silicate melts. *Geochim. Cosmochim. Acta*, 61, 4707–4721.
- Gaye H. and Welfringer J. (1984) Modelling of the thermodynamic properties of complex metallurgical slags. In *Second International Symposium on Metallurgical Slags and Fluxes* (H. A. Fine and D. R. Gaskell, eds.), pp. 357–375. Metallurgical Society AIME.
- Gentile A. L. and Foster W. R. (1963) Calcium hexaluminate and its stability relations in the system CaO-Al₂O₃-SiO₂. *J. Am. Ceramic Soc.*, 46, 74–76.
- Ghiorso M. S. (1994) Algorithms for the estimation of phase stability in heterogeneous thermodynamic systems. *Geochim. Cosmochim. Acta*, 58, 5489–5501.
- Ghiorso M. S. and Sack R. O. (1995) Chemical mass transfer in magmatic processes IV. A revised and internally consistent thermodynamic model for the interpolation and extrapolation of liquid-solid equilibria in magmatic systems at elevated temperatures and pressures. *Contrib. Mineral. Petrol.*, 119, 197–212.
- Göbbels M., Woermann E., and Jung J. (1995) The Al-rich part of the system CaO-Al₂O₃-MgO Part I. Phase relationships. *J. Solid State Chem.*, 120, 358–363.
- Green T. H. (1994) Experimental studies of trace-element partitioning applicable to igneous petrogenesis — Sedona 16 years later. *Chem. Geol.*, 117, 1–36.
- Greenwood H. J. (1975) Thermodynamically valid projections of extensive phase relationships. *Am. Mineral.*, 60, 1–8.

- Grossman J. N., Rubin A. E., and MacPherson G. J. (1988) ALH85085: A unique volatile-poor carbonaceous chondrite with possible implications for nebular fractionation processes. *Earth Planet. Sci. Lett.*, *91*, 33–54.
- Grossman L. (1975) Petrography and mineral chemistry of Ca-rich inclusions in the Allende meteorite. *Geochim. Cosmochim. Acta*, *39*, 433–454.
- Grossman L. (1980) Refractory inclusions in the Allende meteorite. *Annu. Rev. Earth Planet. Sci.*, *8*, 559–608.
- Grossman L., Ebel D. S., Simon S. B., Davis A. M., Richter F. M., and Parsad N. M. (2000) Major element chemical and isotopic compositions of refractory inclusions in C3 chondrites: The separate roles of condensation and evaporation. *Geochim. Cosmochim. Acta*, *64*, 2879–2894.
- Gutt W. (1964) High-temperature phase equilibria for the partial system $3\text{CaO}\cdot\text{MgO}\cdot 2\text{SiO}_2\text{-MgO}\cdot\text{Al}_2\text{O}_3\text{-}2\text{CaO}\cdot\text{Al}_2\text{O}_3\cdot\text{SiO}_2$ in the quaternary system $\text{CaO-SiO}_2\text{-Al}_2\text{O}_3\text{-MgO}$. *J. Iron Steel. Inst.*, *202*, 770–774.
- Gutt W. (1968) Crystallization of merwinite from melilite compositions. *J. Iron Steel. Inst.*, *206*, 840–841.
- Gutt W. and Russell A. D. (1977) Studies of the system $\text{CaO-SiO}_2\text{-Al}_2\text{O}_3\text{-MgO}$ in relation to the stability of blastfurnace slag. *J. Mater. Sci.*, *12*, 1869–1878.
- Hallstedt B. (1990) Assessment of the $\text{CaO-Al}_2\text{O}_3$ system. *J. Am. Ceramic Soc.*, *73*, 15–23.
- Hallstedt B. (1992) Thermodynamic assessment of the system $\text{MgO-Al}_2\text{O}_3$. *J. Am. Ceramic Soc.*, *75*, 1497–1507.
- Hallstedt B. (1995) Thermodynamic assessment of the $\text{CaO-MgO-Al}_2\text{O}_3$ system. *J. Am. Ceramic Soc.*, *78*, 193–198.
- Hallstedt B., Hillert M., Selleby M., and Sundman B. (1994) Modelling of acid and basic slags. *Calphad*, *18*, 31–37.
- Hanson B. and Jones J. H. (1998) The systematics of Cr^{3+} and Cr^{2+} partitioning between olivine and liquid in the presence of spinel. *Am. Mineral.*, *83*, 669–684.
- Hart S. R. and Davis K. E. (1978) Nickel partitioning between olivine and silicate melt. *Earth Planet. Sci. Lett.*, *40*, 203–219.
- Hashimoto A. (1991) Prediction of activities of oxide components in the multicomponent liquid system $\text{FeO-MgO-CaO-Na}_2\text{O-AlO}_{1.5}\text{-SiO}_2$ (abstract). In *Lunar and Planetary Science XXII*, pp. 533–534. Lunar and Planetary Institute, Houston.
- Hewins R. H. and Connolly H. C. Jr. (1996) Peak temperatures of flash-melted chondrules. In *Chondrules and the Protoplanetary Disk* (R. H. Hewins et al., eds.), pp. 197–204. Cambridge Univ., Cambridge.
- Hill E., Wood B. J., and Blundy J. D. (2000) The effect of Ca-Tschermaks component on trace element partitioning between clinopyroxene and silicate melt. *Lithos*, *53*, 203–215.
- Hoover J. D. (1978) The distribution of samarium and thulium between plagioclase and liquid in the systems An-Di and Ab-An-Di at 1300°C. *Carnegie Inst. Wash. Yearb.*, *77*, 703–706.
- Huss G. R., MacPherson G. J., Wasserburg G. J., Russell S. S., and Srinivasan G. (2001) Aluminum-26 in calcium-aluminum-rich inclusions and chondrules from unequilibrated ordinary chondrites. *Meteoritics & Planet. Sci.*, *36*, 975–997.
- Hutcheon I. D., Steele I. M., Smith J. V., and Clayton R. N. (1978) Ion microprobe, electron microprobe and cathodoluminescence data for Allende inclusions with emphasis on plagioclase chemistry. *Proc. Lunar Planet. Sci. Conf. 9th*, pp. 1345–1368.
- Imlach J. A. and Glasser F. P. (1968) Phase equilibria in the system $\text{CaO-Al}_2\text{O}_3\text{-TiO}_2$. *Trans. British Cer. Soc.*, *67*, 581–609.
- Ireland T. R., Fahey A. J., and Zinner E. K. (1991) Hibonite-bearing microspherules: A new type of refractory inclusions with large isotopic anomalies. *Geochim. Cosmochim. Acta*, *55*, 367–379.
- Irving A. J. (1978) A review of experimental studies of crystal/liquid trace element partitioning. *Geochim. Cosmochim. Acta*, *42*, 743–770.
- Ivanova M. A., Petaev M. I., MacPherson G. J., Nazarov M. A., Taylor L. A., and Wood J. A. (2002) The first known occurrence of calcium monoaluminate, in a calcium-aluminum-rich inclusion from the CH chondrite Northwest Africa 470. *Meteoritics & Planet. Sci.*, *37*, 1337–1344.
- Jones J. H. (1995) Experimental trace element partitioning. In *Rock Physics and Phase Relations: A Handbook of Physical Constants, Vol. 3*, pp. 73–104. American Geophysical Union, Washington, DC.
- Jones R. H. (1994) Petrology of FeO-poor, porphyritic pyroxene chondrules in the Semarkona chondrite. *Geochim. Cosmochim. Acta*, *58*, 5325–5340.
- Jones R. H. and Scott E. R. D. (1989) Petrology and thermal history of Type IA chondrules in the Semarkona (LL3.0) chondrite. *Proc. Lunar Planet. Sci. Conf. 19th*, pp. 523–536.
- Kennedy A. K., Lofgren G. E., and Wasserburg G. J. (1994) Trace-element partition coefficients for perovskite and hibonite in meteorite compositions. *Chem. Geol.*, *117*, 379–390.
- Kennedy A. K., Beckett J. R., Edwards D. A., and Hutcheon I. D. (1997) Trace element disequilibria and magnesium isotope heterogeneity in 3655A: Evidence for a complex multi-stage evolution of a typical Allende Type B1 CAI. *Geochim. Cosmochim. Acta*, *61*, 1541–1561.
- Kimura M., El Goresy A., Palme H., and Zinner E. (1993) Ca-, Al-rich inclusions in the unique chondrite ALH85085: Petrology, chemistry, and isotopic compositions. *Geochim. Cosmochim. Acta*, *57*, 2329–2359.
- Kirschen M. and De Capitani C. (1999) Experimental determination and computation of the liquid miscibility gap in the system $\text{CaO-MgO-SiO}_2\text{-TiO}_2$. *J. Phase Equil.*, *20*, 593–611.
- Kirschen M., De Capitani C., Millot F., Rifflet J.-C., and Coutures J.-P. (1999) Immiscible silicate liquids in the system $\text{SiO}_2\text{-TiO}_2\text{-Al}_2\text{O}_3$. *Eur. J. Mineral.*, *11*, 427–440.
- Kohn S. C. and Schofield P. F. (1994) The importance of melt composition in controlling trace-element behaviour: An experimental study of Mn and Zn partitioning between forsterite and silicate melts. *Chem. Geol.*, *117*, 73–87.
- Krigman L. D., Kogarko L. N., and Veksler I. V. (1995) Melilite-melt equilibrium and the role of melilite in the evolution of ultraalkaline magmas. *Geochem. Intl.*, *32*(8), 91–101.
- Krot A. N., Scott E. R. D., and Zolensky M. E. (1995) Mineralogical and chemical modifications of components in CV3 chondrites: Nebular or asteroidal processing? *Meteoritics*, *30*, 748–775.
- Krot A. N., McKeegan K. D., Russell S. S., Meibom A., Weisberg M. K., Zipfel J., Krot T. V., Fagan T. J., and Keil K. (2001) Refractory calcium-aluminum-rich inclusions and aluminum-diopside-rich chondrules in the metal-rich chondrites Hammadah al Hamra 237 and Queen Alexandra Range 94411. *Meteoritics & Planet. Sci.*, *36*, 1189–1216.
- Kuehner S. M., Laughlin J. R., Grossman L., Johnson M. L., and Burnett D. S. (1989) Determination of trace element mineral/liquid partition coefficients in melilite and diopside by ion and electron microprobe techniques. *Geochim. Cosmochim. Acta*, *53*, 3115–3130.

- Kurat G. (1975) Der kohlige Chondrit Lancé: Eine petrologische Analyse der komplexen Genese eines Chondriten. *Tschermaks Mineral. Petrogr.*, 22, 38–78.
- Kushiro I. (1975) On the nature of silicate melt and its significance in magma genesis: Regularities in the shift of the liquidus boundaries involving olivine, pyroxene, and silica minerals. *Am. J. Sci.*, 275, 411–431.
- LaTourrette T. Z. and Burnett D. S. (1992) Experimental determination of U and Th partitioning between clinopyroxene and natural and synthetic basaltic liquid. *Earth Planet. Sci. Lett.*, 110, 227–244.
- Lauretta D. S., Nagahara H., and Alexander C. M. O'D. (2006) Petrology and origin of ferromagnesian silicate chondrules. In *Meteorites and the Early Solar System II* (D. S. Lauretta and H. Y. McSween Jr., eds.), this volume. Univ. of Arizona, Tucson.
- Liang Y., Richter F. M., and Chamberlin L. (1997) Diffusion in silicate melts: III. Empirical models for multicomponent diffusion. *Geochim. Cosmochim. Acta*, 61, 5295–5312.
- Libourel G. (1999) Systematics of calcium partitioning between olivine and silicate melt: Implications for melt structure and calcium content of magmatic olivines. *Contrib. Mineral. Petrol.*, 136, 63–80.
- Lin Y. and Kimura M. (1998) Anorthite-spinel-rich inclusions in the Ningqiang carbonaceous chondrite: Genetic links with Type A and C inclusions. *Meteoritics & Planet. Sci.*, 33, 435–446.
- Lin Y. and Kimura M. (2000) Two unusual Type B refractory inclusions in the Ningqiang carbonaceous chondrite: Evidence for relicts, xenoliths and multi-heating. *Geochim. Cosmochim. Acta*, 64, 4031–4047.
- Lin Y. and Kimura M. (2003) Ca-Al-rich inclusions from the Ningqiang meteorite: Continuous assemblages of nebular condensates and genetic link to Type B inclusions. *Geochim. Cosmochim. Acta*, 67, 2251–2267.
- Longhi J. (1987) Liquidus equilibria and solid solution in the system $\text{Ca}_2\text{Al}_2\text{Si}_2\text{O}_8\text{-Mg}_2\text{SiO}_4\text{-CaSiO}_3\text{-SiO}_2$ at low pressure. *Am. J. Sci.*, 287, 265–331.
- Longhi J. and Pan V. (1988) A reconnaissance study of phase boundaries in low-alkali basaltic liquids. *J. Petrol.*, 29, 115–147.
- Lundstrom C. C., Shaw H. F., Ryerson F. J., Williams Q., and Gill J. (1998) Crystal chemical control of clinopyroxene-melt partitioning in the Di-Ab-An system: Implications for elemental fractionations in the depleted mantle. *Geochim. Cosmochim. Acta*, 62, 2849–2862.
- MacPherson G. J. (2004) Calcium-aluminum-rich inclusions in chondritic meteorites. In *Treatise on Geochemistry, Vol. 1: Meteorites, Comets, and Planets* (A. M. Davis, ed.), pp. 201–246. Elsevier, Oxford.
- MacPherson G. J. and Davis A. M. (1993) A petrologic and ion microprobe study of a Vigarano Type B refractory inclusion: Evolution by multiple stages of alteration and melting. *Geochim. Cosmochim. Acta*, 57, 231–243.
- MacPherson G. J. and Grossman L. (1984) “Fluffy” type A Ca-, Al-rich inclusions in the Allende meteorite. *Geochim. Cosmochim. Acta*, 48, 29–46.
- MacPherson G. J. and Huss G. R. (2000) Convergent evolution of CAIs and chondrules: Evidence from bulk compositions and a cosmochemical phase diagram (abstract). In *Lunar and Planetary Science XXXI*, Abstract #1796. Lunar and Planetary Institute, Houston (CD-ROM).
- MacPherson G. J. and Huss G. R. (2005) Petrogenesis of Al-rich chondrules: Evidence from bulk compositions and phase equilibria. *Geochim. Cosmochim. Acta*, 69, 3099–3127.
- MacPherson G. J., Bar-Matthews M., Tanaka T., Olsen E., and Grossman L. (1983) Refractory inclusions in the Murchison meteorite. *Geochim. Cosmochim. Acta*, 47, 823–839.
- MacPherson G. J., Grossman L., Hashimoto A., Bar-Matthews M., and Tanaka T. (1984a) Petrographic studies of refractory inclusions from the Murchison meteorite. *Proc. Lunar Planet. Sci. Conf. 15th*, in *J. Geophys. Res.*, 89, C299–C312.
- MacPherson G. J., Paque J. M., Stolper E., and Grossman L. (1984b) The origin and significance of reverse zoning in melilite from Allende Type B inclusions. *J. Geol.*, 92, 289–305.
- MacPherson G. J., Wark D. A., and Armstrong J. T. (1988) Primitive material surviving in chondrites: Refractory inclusions. In *Meteorites and the Early Solar System* (J. F. Kerridge and M. S. Matthews), pp. 746–807. Univ. of Arizona, Tucson.
- MacPherson G. J., Petaev M., and Krot A. N. (2004) Bulk compositions of CAIs and Al-rich chondrules: Implications of the reversal of the anorthite/forsterite condensation sequence at low nebular pressures (abstract). In *Lunar and Planetary Science XXXV*, Abstract #1838. Lunar and Planetary Institute, Houston (CD-ROM).
- Maharaj S. V. and Hewins R. H. (1994) Alternative thermal histories for type B Ca-Al-rich inclusions (abstract). In *Lunar and Planetary Science XXV*, pp. 825–826. Lunar and Planetary Institute, Houston.
- Maharaj S. V. and Hewins R. H. (1995) Flash heating a Type B CAI composition (abstract). In *Lunar and Planetary Science XXVI*, pp. 883–884. Lunar and Planetary Institute, Houston.
- Maharaj S. V. and Hewins R. H. (1997) Effect of melt time and precursor phases on type B CAI textures (abstract). In *Lunar and Planetary Science XXVIII*, Abstract #1624. Lunar and Planetary Institute, Houston.
- Malvin D. J. and Drake M. J. (1987) Experimental determination of crystal/melt partitioning of Ga and Ge in the system forsterite-anorthite-diopside. *Geochim. Cosmochim. Acta*, 51, 2117–2128.
- Mason B. and Martin P. M. (1974) Minor and trace element distribution in melilite and pyroxene from the Allende meteorite. *Earth Planet. Sci. Lett.*, 22, 141–144.
- McMurdie H. F. and Insley H. (1936) Studies of the quaternary system $\text{CaO-MgO-2CaO-SiO}_2\text{-5CaO-3Al}_2\text{O}_3$. *J. Res. Nat. Bur. Standards*, 16, 467–474.
- Meeker G. P., Wasserburg G. J., and Armstrong J. T. (1983) Replacement textures in CAI and implications regarding planetary metamorphism. *Geochim. Cosmochim. Acta*, 47, 707–721.
- Mendybaev R. A., Richter F. M., and Davis A. M. (2003) Formation of the melilite mantle of the type B1 CAIs: Experimental simulations (abstract). In *Lunar and Planetary Science XXXIV*, Abstract #2062. Lunar and Planetary Institute, Houston (CD-ROM).
- Miller S. A., Burnett D. S., and Asimov P. D. (2003) Experimental divalent element partitioning between anorthite and CAI melt (abstract). In *Lunar and Planetary Science XXXIV*, Abstract #1446. Lunar and Planetary Institute, Houston (CD-ROM).
- Morse S. A. (1980) *Basalts and Phase Diagrams*. Springer-Verlag, Berlin. 493 pp.
- Nagasawa H., Schreiber H. D., and Morris R. V. (1980) Experimental mineral/liquid partition coefficients of the rare earth

- elements (REE), Sc and Sr for perovskite, spinel and melilite. *Earth Planet. Sci. Lett.*, *46*, 431–437.
- Nash W. P. and Crecraft H. R. (1985) Partition coefficients for trace elements in silicic magmas. *Geochim. Cosmochim. Acta*, *49*, 2309–2322.
- Nurse R. W., Welch J. H., and Majumdar A. J. (1965) The CaO-Al₂O₃ system in a moisture-free atmosphere. *Trans. British Cer. Soc.*, *64*, 409–418.
- O'Neill H. S. C. and Eggins S. M. (2002) The effect of melt composition on trace element partitioning: An experimental investigation of the activity coefficients of FeO, NiO, CoO, MoO₂ and MoO₃ in silicate melts. *Chem. Geol.*, *186*, 151–181.
- Onuma K. and Yagi K. (1967) The system diopside-akermanite-nepheline. *Am. Mineral.*, *52*, 227–243.
- Onuma N., Higuchi H., Wakita H., and Nagasawa H. (1968) Trace element partitioning between two pyroxenes and the host lava. *Earth Planet. Sci. Lett.*, *5*, 47–51.
- Osborn E. F. and Gee K. H. (1969) Part IV. Phase equilibria at liquidus temperatures for a part of the system CaO-MgO-Al₂O₃-TiO₂-SiO₂ and their bearing on the effect of titania on the properties of blast furnace slag. *Bull. Earth Mineral. Sci. Expt. Station*, *85*, 57–80.
- Osborn E. F., DeVries R. C., Gee K. G., and Kraner H. M. (1954) Optimum composition of blast furnace slag as deduced from liquidus data for the quaternary system CaO-MgO-Al₂O₃-SiO₂. *J. Metals (January)*, 3–15.
- Pack A. and Palme H. (2003) Partitioning of Ca and Al between forsterite and silicate melt in dynamic systems with implications for the origin of Ca, Al-rich forsterites in primitive meteorites. *Meteoritics & Planet. Sci.*, *38*, 1263–1281.
- Pan V. and Longhi J. (1989) Low pressure liquidus relations in the system Mg₂SiO₄-Ca₂SiO₄-NaAlSiO₄-SiO₂. *Am. J. Sci.*, *289*, 1–16.
- Pan V. and Longhi J. (1990) The system Mg₂SiO₄-Ca₂SiO₄-CaAl₂O₄-NaAlSiO₄-SiO₂: One atmosphere liquidus equilibria of analogs of alkaline mafic lavas. *Contrib. Mineral. Petrol.*, *105*, 569–584.
- Paque J. M. (1995) Effect of residence time at maximum temperature on the texture and phase compositions of a Type B Ca-Al-rich inclusion analog (abstract). In *Lunar and Planetary Science XXVI*, pp. 1099–1100. Lunar and Planetary Institute, Houston.
- Paque J. M., Beckett J. R., Barber D. J., and Stolper E. M. (1994) A new titanium-bearing calcium aluminosilicate phase: I. Meteoritic occurrences and formation in synthetic systems. *Meteoritics*, *29*, 673–682.
- Paque J. M., Le L., and Lofgren G. E. (1998) Experimentally produced spinel rims on Ca-Al-rich inclusions bulk compositions (abstract). In *Lunar and Planetary Science XXIX*, Abstract #1221. Lunar and Planetary Institute, Houston.
- Paque J. M., Lofgren G. E., and Le L. (2000) Crystallization of calcium-aluminum-rich inclusions: Experimental studies on the effects of repeated heating events. *Meteoritics & Planet. Sci.*, *35*, 363–371.
- Pelton A. D. and Blander M. (1984) Computer-assisted analysis of the thermodynamic properties and phase diagrams of slags. In *Second International Symposium on Metallurgical Slags and Fluxes* (H. A. Fine and D. R. Gaskell), pp. 281–294. Metallurgical Society AIME.
- Pelton A. D., Degterov S. A., Eriksson G., Robelin C., and Dessureault Y. (2000) The modified quasichemical model I — Binary solutions. *Metall. Mater. Trans.*, *31B*, 651–659.
- Peters M. T., Shaffer E. E., Burnett D. S., and Kim S. S. (1995) Magnesium and titanium partitioning between anorthite and Type B CAI liquid: Dependence on oxygen fugacity and liquid composition. *Geochim. Cosmochim. Acta*, *59*, 2785–2796.
- Prigogine I. and Defay R. (1954) *Chemical Thermodynamics*. Longmans, Essex.
- Prince A. T. (1951) Phase equilibrium relationships in a portion of the system MgO-Al₂O₃-2CaO-SiO₂. *J. Am. Ceramic Soc.*, *34*, 44–51.
- Rankin G. A. and Merwin H. E. (1916) The ternary system CaO-Al₂O₃-MgO. *J. Am. Chem. Soc.*, *38*, 568–588.
- Rao M. R. (1968) Liquidus relations in the quaternary subsystem CaAl₂O₄-CaAl₄O₇-Ca₂Al₂SiO₇-MgAl₂O₄. *J. Am. Ceramic Soc.*, *51*, 50–54.
- Rein R. H. and Chipman J. (1963) The distribution of silicon between Fe-Si-C alloys and SiO₂-CaO-MgO-Al₂O₃ slags. *Trans. Metall. Soc. AIME*, *227*, 1193–1203.
- Rein R. H. and Chipman J. (1965) Activities in the liquid solution SiO₂-CaO-MgO-Al₂O₃ at 1600°C. *Trans. Metall. Soc. AIME*, *233*, 415–425.
- Richter F. M., Davis A. M., Ebel D. S., and Hashimoto A. (2002) Elemental and isotopic fractionation of Type B calcium-, aluminum-rich inclusions: Experiments, theoretical considerations, and constraints on their thermal evolution. *Geochim. Cosmochim. Acta*, *66*, 521–540.
- Ringwood A. E. (1975) Some aspects of the minor element chemistry of lunar mare basalts. *Moon*, *12*, 127–157.
- Ryerson F. J. and Hess P. C. (1978) Implications of liquid-liquid distribution coefficients to mineral-liquid partitioning. *Geochim. Cosmochim. Acta*, *42*, 921–932.
- Schairer J. F. (1957) Melting relations of the common rock-forming oxides. *J. Am. Ceramic Soc.*, *40*, 215–235.
- Schairer J. F. and Morimoto N. (1959) The system forsterite-diopside-silica-albite. *Carnegie Inst. Wash. Yearb.*, *58*, 113–118.
- Schairer J. F. and Yoder H. S. (1960) The nature of residual liquids from crystallization, with data on the system nepheline-diopside-silica. *Am. J. Sci.*, *258A*, 273–283.
- Schairer J. F. and Yoder H. S. (1961) Crystallization in the system nepheline-forsterite-silica at one atmosphere pressure. *Carnegie Inst. Wash. Yearb.*, *60*, 141–144.
- Schairer J. F. and Yoder H. S. (1969) Critical planes and flow sheet for a portion of the system CaO-MgO-Al₂O₃-SiO₂ having petrological applications. *Carnegie Inst. Wash. Yearb.*, *68*, 202–214.
- Schairer J. F., Tilley C. E., and Brown G. M. (1967) The join nepheline-diopside-anorthite and its relation to alkali basalt fractionation. *Carnegie Inst. Wash. Yearb.*, *66*, 467–471.
- Schreiber H. D. (1979) Experimental studies of nickel and chromium partitioning into olivine from synthetic basaltic melts. *Proc. Lunar Planet. Sci. Conf. 10th*, pp. 509–516.
- Schreiber H. D., Thanyasiri T., Lach J. J., and Legere R. A. (1978) Redox equilibria of Ti, Cr, and Eu in silicate melts: Reduction potentials and mutual interactions. *Phys. Chem. Glasses*, *19*, 126–139.
- Sheng Y. J. (1992) The origin of plagioclase-olivine inclusions. Ph.D. dissertation, California Institute of Technology, Pasadena.
- Sheng Y. J., Beckett J. R., Hutcheon I. D., and Wasserburg G. J. (1991a) Experimental constraints on the origin of plagioclase-olivine inclusions and CA chondrules (abstract). In *Lunar and Planetary Science XXII*, pp. 1231–1232. Lunar and Planetary Institute, Houston.

- Sheng Y. J., Hutcheon I. D., and Wasserburg G. J. (1991b) Origin of plagioclase-olivine inclusions in carbonaceous chondrites. *Geochim. Cosmochim. Acta*, 55, 581–599.
- Shi P. (1992) Basalt evolution at low pressure: Implications from an experimental study in the system CaO-FeO-MgO-Al₂O₃-SiO₂. *Contrib. Mineral. Petrol.*, 110, 139–153.
- Shi P. and Libourel G. (1991) The effects of FeO on the system CMAS at low pressure and implications for basalt crystallization processes. *Contrib. Mineral. Petrol.*, 108, 129–145.
- Simon S. B. and Grossman L. (2003) Insights into the formation of type B2 refractory inclusions (abstract). In *Lunar and Planetary Science XXXIV*, Abstract #1796. Lunar and Planetary Institute, Houston (CD-ROM).
- Simon S. B., Grossman L., and Davis A. M. (1991) Fassaite composition trends during crystallization of Allende Type B refractory inclusion melts. *Geochim. Cosmochim. Acta*, 55, 2635–2655.
- Simon S. B., Kuehner S. M., Davis A. M., Grossman L., Johnson M. L., and Burnett D. S. (1994a) Experimental studies of trace element partitioning in Ca, Al-rich compositions: Anorthite and perovskite. *Geochim. Cosmochim. Acta*, 58, 1507–1523.
- Simon S. B., Yoneda S., Grossman L., and Davis A. M. (1994b) A CaAl₄O₇-bearing refractory spherule from Murchison: Evidence for very high-temperature melting in the solar nebula. *Geochim. Cosmochim. Acta*, 58, 1937–1949.
- Simon S. B., Davis A. M., and Grossman L. (1996a) A unique ultrarefractory inclusion from the Murchison meteorite. *Meteoritics & Planet. Sci.*, 31, 106–115.
- Simon S. B., Davis A. M., Richter F.-M., and Grossman L. (1996b) Experimental investigation of the effect of cooling rate on melilite/liquid distribution coefficients for Sr, Ba, and Ti in Type B refractory inclusion melts (abstract). In *Lunar and Planetary Science XXVII*, pp. 1201–1202. Lunar and Planetary Institute, Houston.
- Simon S. B., Davis A. M., and Grossman L. (1998) Formation of an unusual compact Type A refractory inclusion from Allende. *Meteoritics & Planet. Sci.*, 33, 115–126.
- Simon S. B., Davis A. M., and Grossman L. (1999) Origin of compact type A refractory inclusions from CV3 carbonaceous chondrites. *Geochim. Cosmochim. Acta*, 63, 1233–1248.
- Soulard H., Provost A., and Boivin P. (1992) CaO-MgO-Al₂O₃-SiO₂-Na₂O (CMASN) at 1 bar from low to high Na₂O contents: Topology of an analogue for alkaline basic rocks. *Chem. Geol.*, 96, 459–477.
- Spear F. S. (1993) *Metamorphic Phase Equilibria and Pressure-Temperature-Time Paths*. Mineralogical Society of America, Washington, DC.
- Srinivasan G., Huss G. R., and Wasserburg G. J. (2000) A petrographic, chemical, and isotopic study of calcium-aluminum-rich inclusions and aluminum-rich chondrules from the Axtell (CV3) chondrite. *Meteoritics & Planet. Sci.*, 35, 1333–1354.
- Steele I. M., Peters M. T., Shaffer E. E., and Burnett D. S. (1997) Minor element partitioning and sector zoning in synthetic and meteoritic anorthite. *Geochim. Cosmochim. Acta*, 61, 415–423.
- Stolper E. (1982) Crystallization sequences of Ca-Al-rich inclusions from Allende: An experimental study. *Geochim. Cosmochim. Acta*, 46, 2159–2180.
- Stolper E. and Paque J. M. (1986) Crystallization sequences of Ca-Al-rich inclusions from Allende: The effects of cooling rate and maximum temperature. *Geochim. Cosmochim. Acta*, 50, 1785–1806.
- Terakado Y. and Masuda A. (1979) Experimental study of REE partitioning between diopside and melt under atmospheric pressure. *Geochem. J.*, 13, 121–129.
- Tingle T. N. (1987) An evaluation of the carbon-14 beta track technique: Implications for solubilities and partition coefficients determined by beta track mapping. *Geochim. Cosmochim. Acta*, 51, 2479–2487.
- Walker D., Shibata T., and DeLong S. E. (1979) Abyssal tholeiites from the Oceanographer Fracture Zone II. Phase equilibria and mixing. *Contrib. Mineral. Petrol.*, 70, 111–125.
- Wark D. A. (1981) The pre-alteration compositions of Allende Ca-Al-rich condensates (abstract). In *Lunar and Planetary Science XII*, pp. 1148–1150. Lunar and Planetary Institute, Houston.
- Wark D. A. (1987) Plagioclase-rich inclusions in carbonaceous chondrite meteorites: Liquid condensates? *Geochim. Cosmochim. Acta*, 51, 221–242.
- Wark D. A., Boynton W. V., Keays R. R., and Palme H. (1987) Trace element and petrologic clues to the formation of forsterite-bearing Ca-Al-rich inclusions in the Allende meteorite. *Geochim. Cosmochim. Acta*, 51, 607–1622.
- Watson E. B. (1976) Two-liquid partition coefficients: Experimental data and geochemical implications. *Contrib. Mineral. Petrol.*, 56, 119–134.
- Watson E. B. (1977) Partitioning of manganese between forsterite and silicate liquid. *Geochim. Cosmochim. Acta*, 41, 1362–1374.
- Weber D. and Bischoff A. (1994) The occurrence of grossite (CaAl₄O₇) in chondrites. *Geochim. Cosmochim. Acta*, 58, 3855–3877.
- Weber D. and Bischoff A. (1997) Refractory inclusions in the CR chondrite Acfer 059 — El Djouf 001: Petrology, chemical composition, and relationship to inclusion populations in other types of carbonaceous chondrites. *Chem. Erde*, 57, 1–24.
- Wood B. J. and Blundy J. D. (2001) The effect of cation charge on crystal-melt partitioning of trace elements. *Earth Planet. Sci. Lett.*, 188, 59–71.
- Wood B. J. and Blundy J. D. (2004) Trace element partitioning under crustal and uppermost mantle conditions: The influences of ionic radius, cation charge, pressure, and temperature. In *Treatise on Geochemistry, Vol. 2: The Mantle and Core* (R. W. Carlson, ed.), pp. 395–424. Elsevier, Oxford.
- Woolum D. S., Johnson M. L., Burnett D. S., and Sutton S. R. (1988) Refractory lithophile partitioning in Type B CAI materials (abstract). In *Lunar and Planetary Science XIX*, pp. 1294–1295. Lunar and Planetary Institute, Houston.
- Yagi K. and Onuma K. (1969) An experimental study on the role of titanium in alkalic basalts in light of the system diopside-akermanite-nepheline-CaTiAl₂O₆. *Am. J. Sci.*, 267-A, 509–549.
- Yoneda S. and Grossman L. (1995) Condensation of CaO-MgO-Al₂O₃-SiO₂ liquids from cosmic gases. *Geochim. Cosmochim. Acta*, 59, 3413–3444.
- Yurimoto H., Rubin A. E., Itoh S., and Wasson J. T. (2001) Non-stoichiometric Al-rich spinel in an ultrarefractory inclusion from CO chondrite (abstract). In *Lunar and Planetary Science XXXII*, Abstract #1557. Lunar and Planetary Institute, Houston (CD-ROM).
- Zen E.-an (1966) *Construction of Pressure-Temperature Diagrams for Multicomponent Systems after the Method of Shreinemakers — A Geometric Approach*. U.S. Geol. Survey Bulletin 1225. 56 pp.
- Zhang S. and Lee W. E. (2000) Use of phase diagrams in studies of refractories corrosion. *Intl. Mater. Rev.*, 45, 41–58.